Designing, optimizing and comparing distributed generation technologies as a substitute system for reducing life cycle costs, CO_2 emissions, and power losses in residential buildings

Delnia Sadeghi[a], Seyed Ehsan Ahmadi[a], Nima Amiri[a], Satinder[a], Mousa Marzband[a,b], Abdullah Abusorrah[b,c], Muhyaddin Rawa[b,c]

[a]*Northumbria University, Electrical Power and Control Systems Research Group, Ellison Place NE1 8ST, Newcastle upon Tyne, UK*
[b]*Center of Research Excellence in Renewable Energy and Power Systems, King Abdulaziz University, Jeddah, 21589, Saudi Arabia*
[c]*Department of Electrical and Computer Engineering, Faculty of Engineering, K. A. CARE Energy Research and Innovation Center, King Abdulaziz University, Jeddah 21589, Saudi Arabia*

Abstract

The optimization of distributed generation technologies and storage systems are essential for a reliable, cost-effective, and secure system due to the uncertainties of Renewable Energy Sources (RESs) and load demand. In this study, two algorithms, the Multi-Objective Particle Swarm Optimization (MOPSO) and the Non-Dominant Sorting Genetic Algorithm II (NSGA-II) were utilized to design five different case studies (CSs) (photovoltaic (PV)/ wind turbine (WT)/ battery/ diesel generator (DG), PV/ WT/ battery/ fuel cell (FC)/ electrolyzer (EL)/ hydrogen tank (HT), PV/ WT/ battery/ grid-connected, PV/ WT/ battery/ grid-connected with Demand Response Program (DRP), and PV/ WT/ battery/ electric vehicle (EV)) to minimize life cycle cost (LCC), loss of power supply probability (LPSP), and CO_2 emissions. In fact, different backups are provided for (PV/ WT/ battery), which is considered as the base system. Further, the uncertainties in RES and load were modeled by the Taguchi method, and Monte Carlo simulation (MCS) was used to model the uncertainties in EV to achieve accurate results. In addition, in CS4, a Demand Response Program (DRP) based on Time-of-Use (TOU) price is considered to study

Email address: mousa.marzband@northumbria.ac.uk Corresponding author (Mousa Marzband)

the effect on the number of specific components and other parameters. Finally, the simulation results verify that the NSGA-II calculation provides accurate and reliable outcomes compared to the MOPSO method, and the PV/WT/battery/ EV combination is the most suitable option among the five designed scenarios.
Keywords: demand response program, electric vehicle, Taguchi method, Monte Carlo simulation, Multi-objective particle swarm optimization, non-dominated sorting genetic algorithm II

Nomenclature

Acronyms

MOPSO	multi-objective particle swarm optimization
NSGA-II	non-dominated sorting genetic algorithm II
CS	case study
PMBSA	pareto multi-objective backtrack search algorithm
PV	photovoltaic
WT	wind turbine
DG	diesel generator
FC	fuel cell
EL	electrolyzer
HT	hydrogen tank
DRP	demand response program
EV	Electric vehicle
LCC	life cycle cost
LPSP	loss of power supply probability
MCS	Monte Carlo simulation
TOU	time of use
MOCS	multi-objective crow search
HS	harmony search
SA	simulated annealing

FPA	flower pollination algorithm
TLBO	teaching-learning based optimization
FHSA	fuzzy harmony search algorithm
IHS	harmony search
SHO	spotted hyena optimization
LIP	load interruption probability
TSA	tunicate swarm algorithm
GDHS	global dynamic harmony search
HGWOSCA	hybrid gray wolf optimizer-sine cosine algorithm

EDF	exponential decreasing function
WEC	wave energy converter
LVF	load variation factor
COE	cost of energy
RF	renewable fraction
NDIWS	non-linearly decreasing inertia weight strategy
CHSLS	cost of hybrid system life span
LOLIP	loss of load interruption probability
LOEE	loss of energy expected
LOLE	loss of load expected
GOA	grasshopper optimization algorithm
NPO	nomadic people optimizer
BMG	biomass generator
TNPC	total system net present cost
TAC	total annual cost
HRES	hybrid renewable energy system
FPA	flower pollination algorithm
ABC	artificial bee colony
IC	initial cost
MC	maintenance cost
SOC	state of charge

Indices

T	index for system lifetime
t	index for time
b	index for battery

Parameters

P_t^L	power demand at time t (kW)
P_t^{PV}	total power produced by the PV modules at a given time t (kW)
P^{stc}	rated power output of PV
G_t^{AC}	solar irradiance in specific environment at particular time t (kW/m^2)
G^{STC}	solar irradiance
T_t^C	temperature of the surface at time t (kW)
T^{STC}	standard temperature
T^a	temperature of the PV location
LCC^{PV}	life cycle cost of the PV ($)
IC^{PV}	initial cost of the PV ($)
MC^{PV}	maintenance cost of the PV ($)
P_t^{WT}	output power of the WT at time t (kW)
P^e	nominal power of the WT
V_t	wind speed at time t (m/s)
V^C	cut-in wind speed (m/s)
V^f	cut-out wind speed (m/s)

V^e	rated speed of the WT (m/s)
LCC^{WT}	life cycle cost of the WT ($)
IC^{WT}	initial cost of the WT ($)
MC^{WT}	maintenance cost of the WT ($)
SOC_t^b	state charge of the battery at time t (kW)
P_t^c	charge power of the battery at time t (kW)
P_t^d	discharge power of the battery at time t (kW)
E^c	rated capacity of the battery
LCC^b	life cycle cost of the battery ($)
IC^b	initial cost of the battery ($)
MC^b	maintenance cost of the battery ($)
RC^b	replacement cost of the battery ($)
P_t^{DG}	output power of the DG at time t (kW)
P^{DGn}	rated power of the DG
f_t^c	fuel consumption of the DG at time t (Liter)
A^{DG}	fuel consumption coefficient of the DG
B^{DG}	fuel consumption coefficient of the DG
P^f	price of fuel
$C^{F,DG}$	fuel cost of the DG
LCC^{DG}	life cycle cost of the DG ($)
IC^{DG}	initial cost of the DG ($)
MC^{DG}	maintenance cost of the DG ($)

RC^{DG}	replacement cost of the DG ($)
$CO2_t^{DG}$	CO_2 emission of DG at time t
LCC^{FC}	life cycle cost of the FC ($)
IC^{FC}	initial cost of the FC ($)
MC^{FC}	maintenance cost of the FC ($)
RC^{FC}	replacement cost of the FC ($)
LCC^{EL}	life cycle cost of the EL ($)
IC^{EL}	initial cost of the EL ($)
MC^{EL}	maintenance cost of the EL ($)
RC^{EL}	replacement cost of the EL ($)
LCC^{HT}	life cycle cost of the HT ($)
IC^{HT}	initial cost of the HT ($)
MC^{HT}	maintenance cost of the HT ($)
RC^{HT}	replacement cost of the HT ($)
P^{price}	cost of power from grid (kWh)
P_t^{grid}	grid power at time t (kW)
$CO_{2_t}^{grid}$	co_2 emissions of grid at time t
$P_t^{L,new}$	final demand after DRP at time t (kW)
T_{arrive}^{EV}	entry time of the EV (t)
T_{dep}^{EV}	leaving time of the EV (t)
SOC_{arrive}^{EV}	SOC at the entry time of the EV (kWh)
SOC_{dep}^{EV}	SOC at the leaving time of the EV (kWh)
Cap^{EV}	capacity of the EV (kWh)
$X_{i,t}$	position of each element in MOPSO
$V_{i,t}$	speed of each element in MOPSO
$Xp_{i,t}$	best position of particle in MOPSO
Xg_t	optimum position of global in MOPSO
	Decision Variables
N^{PV}	quantity PV modules
N^{WT}	quantity WTs
N^b	quantity batteries

N^{DG}	number of DGs
N^{FC}	number of FCs
N^{EL}	number of ELs
N^{HT}	number of HTs

1. Introduction

In the present context, the overexploitation of fossil fuels due to an ever-growing electricity demand would consequently deplete the reserves due to the rapid socio-economic growth leading to an increase in population, urbanization, and technological and industrial advancements. Therefore, supplying the load using traditional methods for generating and transmitting power using large power plants and long transmission lines would increase costs and environmental pollution. Furthermore, conventional power systems experience numerous disadvantages, such as high costs, redesign, increased demand, losses, fluctuations, and so on. Therefore, decision-makers and stakeholders of existing power systems are required to provide novel and cost-effective solutions to mitigate these issues. For this reason, distributed energy sources have been suggested to meet the load demand, reduce carbon emissions, and operate efficiently at lower costs [1–4]. Also, EVs are gaining popularity because they do not emit tailpipe pollutants, are more efficient, operate quietly, and are eco-friendly as compared to internal combustion engines. However, EVs could cause heavy grid stress when connected to the network when charging, especially during peak hours [5, 6]. Hence, by implementing the properly planned controlled infrastructure, EVs could be applied as energy sources to supply and meet load demand [7–9].

1.1. Literature review and contributions

Several studies have been investigated to implement the optimal infrastructure in the literature. For instance, in [10], the flower pollination algorithm (FPA), teaching-learning based optimization (TLBO), and PSO are used to optimally design renewable energy systems that include PV, WT, FC, EL, and HT. In this research, different scenarios of PV/ FC, PV/ WT/ FC, and WT/ FC have been investigated by

considering the net present cost (NPC), loss of energy expected (LOEE), and loss of load expected (LOLE) indices. In fact, the results show that the PV/ WT/ FC system has lower cost and higher reliability in different weather conditions, and the FPA algorithm performs better than the other two algorithms in terms of accuracy and speed of convergence. In [11], the authors have applied the fuzzy harmony search algorithm (FHSA) and HSA to optimize the PV/ WT/ battery/ DG system in different cases, in which PV and WT are the main sources, while DG and battery play the backup roles. Moreover, the loss of power supply probability (LPSP), total annual cost (TAC), and the sensitivity analysis on LPSP in different scenarios have been examined. Consequently, the results confirm that the FHSA algorithm performs better than the HSA, and a backup system could save up to 24%. The independent PV/ battery system has been studied in the literature [12] using improved harmony search (IHS), simulated annealing (SA), and HS algorithms considering LCC and LPSP indices. The results concluded that the IHS algorithm is the most suitable option. In [13, 14], spotted hyena optimization (SHO) and PSO algorithms are used to design different cases of PV/ battery, PV/ WT/ battery, and WT/ battery, which are off-grid and on-grid. In this study, load interruption probability (LIP) and NPC indices are considered. In [15], the tunicate swarm algorithm (TSA) is proposed to solve the problem of optimizing an independent micro-grid, which includes PV, WT, battery, and DG, designed to power a remote village in Egypt with the goals of LPSP, COE, NPC, and TAC. In [16], two Pareto multi-objective backtrack search algorithm (PMBSA) and NSGA-II algorithms are used to obtain the best configuration of the independent hybrid renewable energy system. This system has been studied in two different scenarios: PV/ WT/ battery/ DG and PV/ WT/ battery/ DG/ biomass generator (BMG), considering the objectives of LCC, LPSP, CO2, and dump load. In [17], three improved versions of global dynamic harmony search (GDHS) have been used to design an independent hybrid WT/ hydrogen system with the aim of reducing costs and increasing reliability. Finally, the results show that the proposed algorithm optimizes renewable energy systems with fast convergence and high accuracy. In [18], a new hybrid meta-heuristic algorithm called the hybrid grey wolf optimizer-sine cosine algorithm (HGWOSCA) based on exponential decreas-

ing function (EDF) for the optimal and cost-effective design of three hybrid systems, PV/ FC, PV/ WT/ FC, and WT/ FC is used. Finally, the results of this algorithm are compared with the results of GWO, SCA, and PSO, and it is shown that HGWOSCA has better performance than the other three algorithms. In [19], two different hybrid systems along with an electric vehicle were considered, the first system is the combination of PV/ WT/ battery and the other system is combined with PV/ WT/ battery/ EV. In the first system, the numbers of excellent items and distinct prices at different LPSP levels were first attained, and then the EV was added to the system, considering their deterministic and stochastic behavior. Additionally, LPSP has been recomputed in both inevitable and probable states, and EV has been demonstrated to increase the system's security. In the next system, the effects of the inevitable and then statistically probable performance of the EV on the number of components and LPSP were investigated at the initial stage. In [20], optimal size and power exchange of a grid-connected DG/ PV/ FC hybrid system was investigated by a multi-objective crow search (MOCS) algorithm for a community in Kerman, Iran with the aim of LPSP and LCOE. In [7], a grid-independent micro-grid consisting of PV/ WT/ battery with and without a demand response program was investigated using both GAMZ and HOMER software. The authors in [21], used HS and SA algorithms to optimize a PV/ battery system, with the purpose of reducing the price and increasing the reliability. In [22], the HOMER software was adopted to enhance the PV/ WT/ Wave Energy Converter (WEC) system to supply electricity for 10,000 residents living in coastal areas. In [23, 24], HS, Jaya, and PSO algorithms were used in determining the best model size of a combined power system containing a set of the PV/ WT/ battery to effectively meet customers' cost-effectiveness, reliability, and electricity demands. In [25], the size optimization of the PV/ DG hybrid system was performed by considering the demand response program and the goals of TNPC and LPSP using two algorithms, MOPSO and MOCS. Consequently, in this study, a new indicator called load variation factor (LVF) was defined, which determines the amount of reduced load during peak hours to provide a more economical system. The authors [26], used the PSO and constraint method to improve a DG/ PV/ WT/ battery model in which the objectives were to reduce the cost of energy

(COE) and increase reliability and a renewable fraction (RF) for providing electrical energy to provincial buildings. In [27], a techno-budgetary and real analysis of an independent hybrid model, including WEC/ PV/ WT/ battery, was carried out in three different regions of Iran to supply electricity to 3,000 residential houses. In [28], the PV/ WT/ FC arrangement for a distant location in Iran was optimized using an improved meta-heuristic sine-cosine algorithm (ISCA) established on a decreasing nonlinear inertia weight strategy (NDIWS) aimed at reducing the cost of hybrid system life span (CHSLS) and loss of load interruption probability (LOLIP). In [29], five different scenarios (PV/ battery, WT/ battery, single DG, 3-split DG, PV/ WT/ Split-DG/ battery) were examined, employing a multi-purpose GA which is intended to reduce CO2, LCC, and discarded energy. In [30], authors proposed the Grasshopper Optimization Algorithm (GOA) to improve the PV/ WT/ battery/ DG system, which was intended to address the deficiency of power supply probability (DPSP) and COE. In [31], authors analyzed six different scenarios (PV/ battery, WT/ battery, one large DG, 20-split DG, PV/ WT/ Split-DG/ battery, PV/ WT/ one large DG/ battery) were examined employing a multi-purpose Nomadic People Optimizer (NPO) aiming to decrease CO2, LCC, and discharge power, a PV/ WT/ single large DG/ battery model is excellent. In [32], a PV/ WT was constructed with and without consideration for a backup system, in which the goals were to decrease energy prices and strengthen security. In [33], different scenarios (PV/ WT/ BMG/ biogas generator (BGG)/ FC/ battery, PV/ WT/ BMG/ BGG/ FC, PV/ WT/ BMG/ BGG/ battery, and PV/ WT/ BMG/ BGG) were evaluated using HOMER software and Genetic Algorithm (GA) to electrify three suburbs in Kollegal, a subdivision of Chamarajanagar district, Karnataka, India, with the goals of Total System Net Preset Cost (TNPC), COE, unfulfilled demand, and CO_2 discharges. In [34], MG including PV/ WT, is designed using HOMER charging station software to reduce cost. In [35–38], several HRES systems have been improved using HOMER software. In [39], the size and design of the grid-connected system, including PV/ WT/ FC, were optimized to supply a recreational place load in Egypt using Hybrid Firefly (HFA), HS, and PSO with LPSP, COE, and TNPC targets. In [40], the GA was used to optimize the size of the grid-connected PV/ battery system to reduce

costs. In [41], a grid-based PV/ WT energy system was designed with PSO to reduce costs. Authors in [42], used the Flower Pollination Algorithm (FPA) to optimize the independent PV/ FC model and were targeted at reducing LPSP and COE. Consequently, the outcomes of FPA were correlated with the outputs of an artificial bee colony (ABC) and PSO, and it was found that the FPA performed better than the alternatives. Researchers in [43], have provided a comprehensive review of modern optimization methods and techniques for hybrid energy systems, including PV/ DG/ storage systems. In [44, 45], a comprehensive review of multi-objective optimization (MOO) and multi-criteria decision-making (MCDM) methodologies for standalone photovoltaic (SAPV) systems was conducted to assist designers in selecting the most appropriate design before installing a SAPV system. In [46, 47], a complete overview of the most popular tools and the most important objectives taken into consideration in HRES, which provides the designer's valuable information to better design HRES technically and economically. In [48], the WT/ DG/ battery hybrid model, which investigates the performance of three categories of batteries for a specific territory in China, was inspected. In this study, 280 houses were considered while acknowledging the NPC, COE, and emissions indicators applicable to Homer. In [49, 50], off-grid HRESs were created and uncertainty models were also modeled for PV and WT renewable sources using Monte Carlo simulation.

The contrast between the suggested systems in this research and the models presented in the existing research is outlined in Table 1. Although, the existing researches have suggested various ways to create and improve HRESs, none of them have considered the EV as a backup for HRESs. Therefore, in this paper, to increase system reliability and reduce operating costs and pollution, the idea of considering EV as support for HRESs with other support modes is presented. The main contributions of this article could be listed as follows:

- ✓ Size optimization problem modeling utilizing MOPSO and NSGA-II for grid-connected and independent HRESs with simultaneous consideration of LCC, LPSP, and CO_2 emissions objectives.
- ✓ Modelling the uncertainty of EV parameters using MCS as well as renewable and load sources using the Taguchi method in the size optimization problem.

✓ Modelling different backup modes and comparing with the EV while considering the DRP in the problem.

Table 1: Comparison between existing and proposed HRES designs

Reference	HRES's Resources	Considering DRP	Uncertainty	Utilized Method or tools	On/Off grid
[19]	PV, WT, and battery	No	No	MOPSO and MCS	off
[25]	PV and DG	Yes	-	MOPSO and MOCS	off
[20]	PV, DG, and FC	No	-	MOCS	on
[7]	PV, WT, and battery	Yes	-	HOMER and GMZ	off
[50]	PV, WT, and battery	No	PV and WT	NSGA-II and MCS	off
[33]	PV, WT, BMG, BGG, FC, and battery	No	-	HOER and GA	off
[31]	PV, WT, Split-DG, and battery	No	-	NPO	off
[40]	PV and battery	No	-	GA	on
[22]	PV, WT, and WEC	No	-	HOMER	on
Our study	PV, WT, battery, DG, FC, EL, FC, and EV	Yes	PV, WT, load, and EV	MOPSO, NSGA-II, MCS, and Taguchi	Off grid and on grid

2. Problem Description

The optimal sizing of HRESs is currently receiving much attention, and researchers have worked extensively to evaluate innovative methods to minimize expenditure and pollution while improving security. In several articles, for example, [29, 31], they looked at different HRES system design scenarios, considering different PV/ WT/ battery system backups, and compared them in different aspects to acquire the best option. However, in none of the research done so far, researchers haven't compared EV as a backup system with other systems, whereas this issue is raised in this article.

The HRESs studied in this paper include PV, WT, battery, DG, FC, EL, HT, and EV, the structure of which is shown in Figure 1. In fact, in this article, five different CSs were considered to examine the different backup modes of PV/ WT/ battery systems. In this regard, the uncertainty in solar irradiance, wind speed, and the required demand is modeled using the Taguchi method, while the uncertainty in the behavior of the EV owner is modeled using the MCS. Further, in CS4, a DRP is considered to examine its impact on the number of selected components and other parameters.

For this study, the decision variables are a perfect number of units, which are PV, WT, battery, DG, FC, EL, HT, and grid power. Additionally, the MOPSO and NSGA-II algorithms are applied to optimize the number of units in the hybrid systems for a typical household in Sanandaj city by considering the three objective functions LPSP, LCC, and co_2. Further, the inputs to the problem under study could be identified as data on load, wind speed, solar radiation, and economic parameters.

3. Mathematical Formulation

This section consists of individual subsections for every element of the HREs, which are mathematically formulated, and every computation is demonstrated over the lifespan of the research. Accordingly, the objective functions and constraints are described.

3.1. The PV model

The power output of the PV system depends on the module specifications and the changes in the surroundings. And it doesn't need mechanical or chemical devices to produce power. The power produced by the PV modules is calculated by equation (1) [19, 51]:

$$P_t^{PV} = P^{STC}\eta\left(\frac{G_t^{AC}}{G^{STC}}\right)\left[1+\alpha\left(T_t^C - T^{STC}\right)\right] \tag{1}$$

$$T_t^C = T^a + \frac{NOCT-20}{800}G^{AC} \tag{2}$$

In the above equations, P_t^{PV}, is the power produced by the PV, P^{STC} is the rated power, and η defines the surface contamination limiting coefficient of the solar panel varied between 0.9 and 0.95. G^{STC}, is the light intensity, G_t^{AC} corresponds to light strength in a specific environment, α corresponds to the temperature coefficient of power, T^{STC} is the standard temperature, and T_t^C defines the panel's exterior temperature. In equation (2), T^a relates to the temperature at the panel site, and $NOCT$ is fluctuating between 0 and 2° C.

The life cycle cost (LCC^{PV}) related to PV consists initial cost (IC^{PV}) and maintenance cost (MC^{PV}), obtained from equations (3) to (5) [52]:

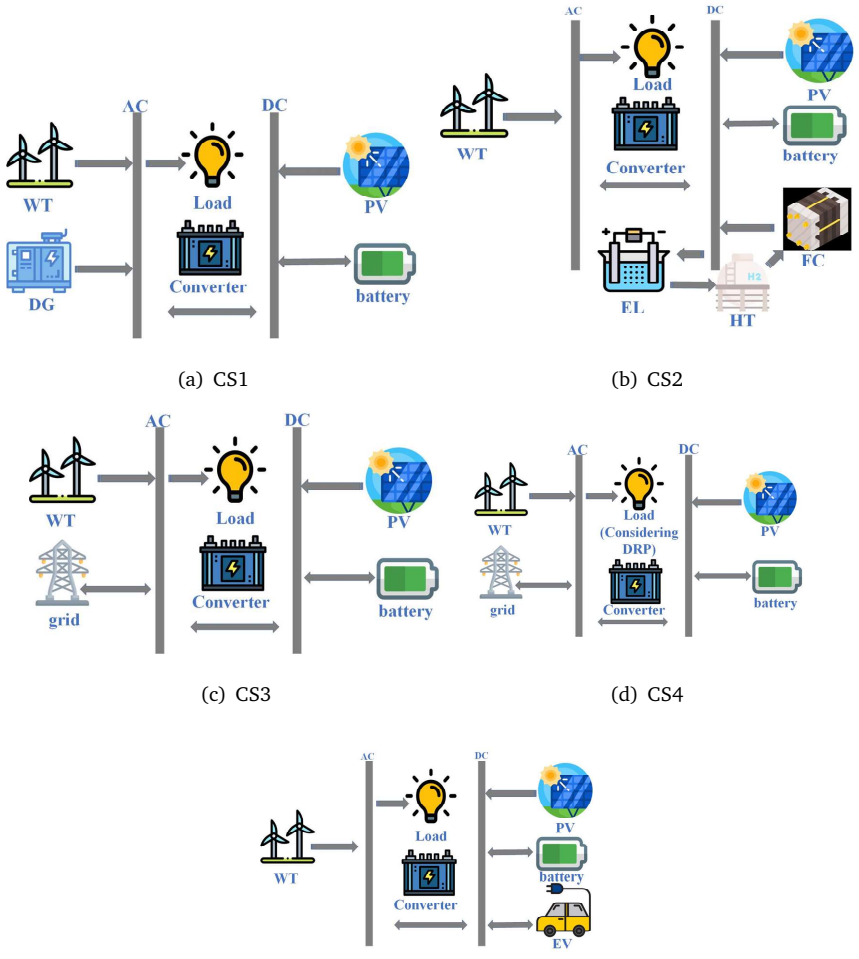

Figure 1: Structure of HRESs for (a) CS1, (b) CS2, (c) CS3, (d) CS4, and (e) CS5

$$LCC^{PV} = IC^{PV} + MC^{PV} \tag{3}$$

$$IC^{PV} = (C_I^{PV} \times N^{PV}) \tag{4}$$

$$MC^{PV} = \left(C_M^{PV} \times N^{PV}\right) \sum_{t=1}^{T} \left(\frac{1 + InfR}{1 + IntR}\right)^t \tag{5}$$

where, N^{PV} is the number of PVs, and T corresponds to the lifespan of the system, $InfR$ is the rate of inflation while $IntR$ is the rate of interest.

3.2. The WT model

Wind energy is the most common renewable source used for power production, whereby the WT model and climatic conditions decide its output. The WT output power produced hourly is computed by equation (6) [19, 53] refers to the speed of wind:

$$P_t^{WT} = \begin{cases} P^e \frac{V_t^c - V^c}{V^e - V^c} & V^c \leqslant V_t < V^e \\ P^e & V^e \leqslant V_t \leqslant V^f \\ 0 & V_t \leqslant V^c \text{ or } V_t \geqslant V^f \end{cases} \tag{6}$$

where, P_t^{WT} is the output power of the WT, P^e refers to the rated power output of every WT, V_t corresponds to the speed of the wind, V^c refers to break-in speed, V^f is stopping speed, and V^e refers to the WT's nominal speed in meters per second. The LCC^{WT} of the WT includes IC^{WT} and MC^{WT}, obtained from equations (7) to (9) [52]:

$$LCC^{WT} = IC^{WT} + MC^{WT} \tag{7}$$

$$IC^{WT} = (C_I^{WT} \times N^{WT}) \tag{8}$$

$$MC^{WT} = \left(C_M^{WT} \times N^{WT}\right) \sum_{t=1}^{T} \left(\frac{1 + InfR}{1 + IntR}\right)^t \tag{9}$$

3.3. The battery model

The battery charges during low demand hours and supplies extra energy when demand is higher. Equation (10) and (11) demonstrates the process of charging and discharging [19, 54]:

Charging mode:

$$SOC_t^b = (1-\delta)\, SOC_{(t-1)} - P^c \mu^c \Delta t / E^c \tag{10}$$

Discharging mode:

$$SOC_t^b = (1-\delta)\, SOC_{(t-1)} - P_t^d \Delta t / E^c \ \mu^d \tag{11}$$

According to Eqs. (10)- (11), SOC indicates the charging mode, E^c is the nominal capacity, δ is the rate of discharging, μ^c and μ^d refers to coefficients of charging and discharging, respectively, while P_t^c and P_t^d are the charge and discharge power, respectively.

The $LCC^b$of the battery includes IC^b, MC^b, and replacement cost (RC^b), obtained from equations (10) to (13) [55]:

$$LCC^b = IC^b + MC^b + RC^b \tag{12}$$

$$IC^b = (C_I^b \times N^b) \tag{13}$$

$$MC^b = \left(C_M^b \times N^b\right) \sum_{t=1}^{T} \left(\frac{1+Inf R}{1+Int R}\right)^t \tag{14}$$

$$RC^b = \left(C_R^b \times N^b\right) \sum_{t=1}^{T} \left(\frac{1+Inf R}{1+Int R}\right)^t \tag{15}$$

where, N_n^b is the number of batteries, and it is presumed to change the battery after several life cycles which indicates in equation (12).

3.4. The DG model

When the demand is high and the power generated by renewable sources is not sufficient to meet demand, the DG system performs as a backup.

Diesel used by DG (f_t^c) depends on fuel consumption coefficients ($A^{DG}$and B^{DG}), the power generated by the DG every hour (P_t^{DG}), and the rated power of DG (P^{DGn}), is obtained from equation (16) [20, 29]:

$$f_t^c = A^{DG} \times P^{DGn} \ + B^{DG} \times P_t^{DG} \tag{16}$$

When the DG is working, the amount of diesel used is computed by equation (16). Fuel usage is zero when DG is not in use. Further, the fuel price of diesel generator, ($C^{F,DG}$) rely on cost of diesel (P^f), obtained from equation (17):

$$C_t^{fuel} = P^f \times f_t^c \tag{17}$$

$$C^{F,DG} = \sum_{1}^{T} C_t^{fuel} \tag{18}$$

By considering fuel cost ($C^{F,DG}$), IC^{DG}, MC^{DG} and RC^{DG}, LCC of diesel generator (LCC^{DG}) could be calculated as follows:

$$LCC^{DG} = IC^{DG} + MC^{DG} + RC^{DG} \times RC^{F,DG} \tag{19}$$

$$IC^{DG} = (C_I^{DG} \times N^{DG}) \tag{20}$$

$$MC^{DG} = \left(C_M^{DG} \times N^{DG}\right) \sum_{t=1}^{T} \left(\frac{1+InfR}{1+IntR}\right)^t \tag{21}$$

$$RC^{DG} = \left(C_R^{DG} \times N^{DG}\right) \sum_{t=1}^{T} \left(\frac{1+InfR}{1+IntR}\right)^t \tag{22}$$

$$RC^{F,DG} = C^{F,DG} \times \sum_{t=1}^{T} \left(\frac{1+InfR}{1+IntR}\right)^t \tag{23}$$

The co_2 emission of a DG at time t is related to its fuel consumption, which is obtained from equation (24):

$$CO_{2t}^{DG} = S_{CO_2}^{DG} \times f_t^c \tag{24}$$

where, $S_{CO_2}^{DG}$ is the specific emissions of carbon dioxide per liter of fuel, given as 2.7 kg/l

3.5. The FC model

A fuel cell is an apparatus that transforms energy to generate electricity continuously by supplying oxygen to the anode and hydrogen to the cathode.

The LCC^{FC} of the FC includes IC^{FC}, MC^{FC}, and RC^{FC}, obtained from equations (25) to (28) [20, 25]:

$$LCC^{FC} = IC^{FC} + MC^{FC} + RC^{FC} \tag{25}$$

$$IC^{FC} = (C_I^{FC} \times N^{FC}) \tag{26}$$

$$MC^{FC} = \left(C_M^{FC} \times N^{FC}\right) \sum_{t=1}^{T} \left(\frac{1+InfR}{1+IntR}\right)^t \tag{27}$$

$$RC^{FC} = \left(C_R^{FC} \times N^{FC}\right) \sum_{t=1}^{T} \left(\frac{1+InfR}{1+IntR}\right)^t \tag{28}$$

where, N^{FC} is the number of FC and, the FC required to be restored is presumed, as considered in equation (25).

3.6. The EL model

The process of water break down water into oxygen and hydrogen gas by supplying electrical current is known as water electrolysis. In fact, the generated hydrogen by EL is perfect for FCs utilization. Hydrogen is produced in an adequate amount to be stock in HTs and utilized when there is a deficiency.

The LCC^{EL} of the EL includes IC^{EL}, MC^{EL}, and RC^{EL}, obtained from equations (29) to (32) [20, 25]:

$$LCC^{EL} = IC^{EL} + MC^{EL} + RC^{EL} \tag{29}$$

$$IC^{EL} = (C_I^{EL} \times N^{EL}) \tag{30}$$

$$MC^{EL} = \left(C_M^{EL} \times N^{EL}\right) \sum_{t=1}^{T} \left(\frac{1 + InfR}{1 + IntR}\right)^t \tag{31}$$

$$RC^{EL} = \left(C_R^{EL} \times N^{EL}\right) \sum_{t=1}^{T} \left(\frac{1 + InfR}{1 + IntR}\right)^t \tag{32}$$

where, N^{EL} is the number of EL and, the restoration of EL is presumed, as shown in equation (29).

3.7. The HT model

The hydrogen produced by the EL is stored in HTs. The LCC^{HT} of the HT includes IC^{HT} and MC^{HT} obtained from Equations (33) to (35) [20, 25]:

$$LCC^{HT} = IC^{HT} + MC^{HT} \tag{33}$$

$$IC^{HT} = (C_I^{HT} \times N^{HT}) \tag{34}$$

$$MC^{HT} = \left(C_M^{HT} \times N^{HT}\right) \sum_{t=1}^{T} \left(\frac{1 + InfR}{1 + IntR}\right)^t \tag{35}$$

3.8. The grid model

The grid is used as a backup power source and to produce power during periods when the output power of PV and WT is not sufficient to meet demand [51]. When grid power is more than zero, electricity buys from of the grid, and when grid power is less than zero, the grid buys electricity, which is obtained from equation (36).

$$COE = P^{price} \sum_{t=1}^{T} P_t^{grid} \times t \tag{36}$$

where, COE is the cost of energy, P_t^{grid} denotes grid power, P^{price} is the cost of energy per kWh, and t is the sampling time. The grid's carbon dioxide emission at time t is related to its fuel consumption, which is obtained from equation (37):

$$CO_{2t}^{grid} = S_{CO_2}^{grid} \times P_t^{grid} \tag{37}$$

For every KWh, carbon dioxide emissions in grams per KWh, $S_{CO_2}^{grid}$, which is equal to 230.7 [56].

3.9. The DRP model

In this study, the DRP-based time of use (TOU) price was considered. The DRP based on TOU motivates the utilization control of consumers as per the cost indication received. Hence, consumers want to decrease their consumption when the cost is high or turn lower cost time periods.

According to specifications of load inclusive of load description and elasticity in price, in [57, 58] researchers have observed a global economic system that is responsive to demand, which is the system designed and built on the TOU cost given in equation (38).

$$P_t^{L,new} = P_t^L \times \left\{ 1 + \frac{E_t . \left[P_t^{price,new} - P_t^{price} \right]}{\rho_t} + \sum_{\substack{h=1 \\ h \neq t}}^{24} E_{t,h} . \frac{P_t^L}{\rho_h} \left[P_h^{price,new} - P_t^{price} \right] \right\} \forall\, t \neq h \tag{38}$$

where, P_t^L is the initial demand, $P_t^{L,new}$ is the final demand, P_t^{price} and $P_t^{price,new}$ are the initial and final prices respectively, while E_t and $E_{t,h}$ are self and elasticity across the self, accordingly.

3.10. The EV model

The EV battery is similar to a regular battery with several additional parameters such as T^{EV}_{arrive} , T^{EV}_{dep} , SOC^{EV}_{arrive} , and SOC^{EV}_{dep} charged and discharged, respectively.

According to [19], the EV's arriving time, leaving time, and SOC at entry follow a normal function of distribution. however, an inequality constraint for the EV's SOC at leaving time has been considered in this paper.

$$T^{EV}_{arrive} \sim N\left(\mu^{EV}_{a}, \sigma^{EV}_{a}\right) \tag{39}$$

$$T^{EV}_{dep} \sim N\left(\mu^{EV}_{d}, \sigma^{EV}_{d}\right) \tag{40}$$

$$SOC^{EV}_{arrive} \sim N\left(\mu^{EV}_{a}, \sigma^{EV}_{a}\right) \tag{41}$$

$$SOC^{EV}_{dep} \geqslant 0.2 \times Cap^{EV} \tag{42}$$

where, T^{EV}_{arrive} and T^{EV}_{dep} corresponds to the EV's entry and leaving time, respectively. SOC^{EV}_{arrive} and SOC^{EV}_{dep} refers to the EV's SOC at the entry and leaving, respectively. The parameters, μ and σ refers to the mean and standard deviation, respectively, and Cap^{EV} is EV's capacity. It is assumed that the departure SOC of the EV is not less than 20% the EV capacity

3.11. Objective functions

✓ Life Cycle Cost (LCC):

The total life cycle cost (TLCC) of the model is the expenditure during the lifespan of the system. In fact, sizing problem's objective function is described by equation (43) to (46), to reduce TLCC for each case study:

CS1 (PV/ WT/ battery/ DG):

$$TLCC = LCC^{PV} + LCC^{WT} + LCC^{b} + LCC^{DG} \tag{43}$$

CS2 (PV/ WT/ battery/ FC/ EL/ HT):

$$TLCC = LCC^{PV} + LCC^{WT} + LCC^{b} + LCC^{FC} + LCC^{EL} + LCC^{HT} \tag{44}$$

CS3 (PV/ WT/ battery/ grid-connected) and CS4 (PV/ WT/ battery/ grid-connected with DRP):

$$TLCC = LCC^{PV} + LCC^{WT} + LCC^{b} + COE^{grid} \tag{45}$$

CS5 (PV/ WT/ battery/ EV):

$$TLCC = LCC^{PV} + LCC^{WT} + LCC^{b} \tag{46}$$

✓ Loss of Power Supply Probability (LPSP):

LPSP corresponds to the proportion of the shortage in power supply and the requirement of active load for a definite time duration as demonstrated in equations (47) to (51) for each case study.

CS1 (PV/ WT/ battery/ DG):

$$f^{LPSP} = \frac{\sum_{j=1}^{8760}\left[P_t^L - \left(P_t^{WT} + P_t^{PV} + P_t^b + P_t^{DG}\right)\right]}{\sum_{j=1}^{8760} P_t^L} \tag{47}$$

CS2 (PV/ WT/ battery/ FC/ EL/ HT):

$$f^{LPSP} = \frac{\sum_{j=1}^{8760}\left[P_t^L - \left(P_t^{WT} + P_t^{PV} + P_t^b + P_t^{FC}\right)\right]}{\sum_{j=1}^{8760} P_t^L} \tag{48}$$

CS3 (PV/ WT/ battery/ grid-connected):

$$f^{LPSP} = \frac{\sum_{j=1}^{8760}\left[P_t^L - \left(P_t^{WT} + P_t^{PV} + P_t^b + P_t^{grid}\right)\right]}{\sum_{j=1}^{8760} P_t^L} \tag{49}$$

CS4 (PV/ WT/ battery/ grid-connected with DRP):

$$f^{LPSP} = \frac{\sum_{j=1}^{8760}\left[P_t^{L,new} - \left(P_t^{WT} + P_t^{PV} + P_t^b + P_t^{grid}\right)\right]}{\sum_{j=1}^{8760} P_t^{L,new}} \tag{50}$$

CS5 (PV/ WT/ battery/ grid-connected with DRP):

$$f^{LPSP} = \frac{\sum_{j=1}^{8760}\left[P_t^L - \left(P_t^{WT} + P_t^{PV} + P_t^b + P_t^{EV}\right)\right]}{\sum_{j=1}^{8760} P_t^L} \tag{51}$$

where, P_t^L represents the load, P_t^{WT}, P_t^{PV}, P_t^b, P_t^{EV}, P_t^{DG}, P_t^{FC}, and P_t^{grid} represent the output power of WT, PV, battery, EV, DG, FC, and grid, respectively.

✓ CO_2 emissions:

Pollution is only produced in CS1, CS3, and CS4. The emission of co_2 in a DG and grid throughout the lifespan of the model is the summation of all hourly co_2 emissions, which is obtained from equations (52) to (53).

CS1 (PV/ WT/ battery/ DG)

$$CO_{2_t}^{total,DG} = \sum_{t=1}^{T} CO_{2_t}^{DG} \tag{52}$$

CS3 (PV/ WT/ battery/ grid-connected) and CS4 (PV/ WT/ battery/ grid-connected with DRP):

$$CO_{2_t}^{total,grid} = \sum_{t=1}^{T} CO_{2_t}^{grid} \tag{53}$$

3.12. Equality and inequality limitations

The suggested objective functions have been improved. The technical limitations, and the constraints are described as follows:

$$SOC^{min} \leqslant SOC_t \leqslant SOC^{max} \tag{54}$$

$$P^{grid\ min} \leqslant P^{grid} \leqslant P^{grid\ max} \tag{55}$$

Equation (54) shows the charge level per hour must not have a lower value than the least value or a higher value than the highest value, and the power limits of the grid are demonstrated by equation (55).

$$N^{min} \leqslant N^{PV} \leqslant N^{max} \tag{56}$$

$$N^{min} \leqslant N^{WT} \leqslant N^{max} \tag{57}$$

$$N^{min} \leqslant N^{b} \leqslant N^{max} \tag{58}$$

$$N^{min} \leqslant N^{DG} \leqslant N^{max} \tag{59}$$

$$N^{min} \leqslant N^{FC} \leqslant N^{max} \tag{60}$$

$$N^{min} \leqslant N^{EL} \leqslant N^{max} \tag{61}$$

$$N^{min} \leqslant N^{HT} \leqslant N^{max} \tag{62}$$

Equations (56) to (62) show the limitations of the numerous mixed system elements, where N^{PV} refers to count of PVs, N^{WT} is the WTs' counts, N^{b} is the batteries' count, N^{DG} is the DGs' count, N^{FC} is the FCs count and N^{EL} is the ELs' count, N^{HT} is the count of HTs, respectively,

4. Solving Procedure

4.1. MOPSO

MOPSO algorithm actions are given as below [19, 59].

1. The first residents are created.

2. Every particle decides its new position using two weighted functions. One looks for a difference between the present position and a better position among all the iterations. The other function measures the difference between the present and the leader's position. This section is similar to PSO, and the velocity and position vectors of every particle are modified based on equations (63) to (64).

$$v_{i,(t+1)} = w \times v_{i,t} + c_1 r_1 \left(xp_{i,t} - x_{i,t}\right) + c_2 r_2 \left(xg_t - x_{i,t}\right) \tag{63}$$

$$x_{i,(t+1)} = x_{i,t} + v_{i,(t+1)} \tag{64}$$

   Where, $x_{i,t}$ shows the particle i^{th} position at an instance t, and $v_{i,t}$ indicates the velocity of the i^{th} particle at the same moment. In addition, the parameters r_1 and r_2 are variables which are random, c_1 and c_2 represent the weighting constants, and w is the weight of inertia.

3. A dominant rule has been created for dual or more objective functions as mentioned under.

   Rule: x_1 (solution 1) is superior to x_2 (solution 2) if:

   a. $f_i(x_1) \leqslant f_i(x_2)$ for all the objective functions 1 to i.

   b. $f_i(x_1) < f_i(x_2)$ for at least one objective function 1 to i.

4. The leader is selected based on the same attribute as all non-dominant particles, whereas the most powerful particle is selected as the leader.

5. Non-dominant citizens are isolated from the population and stored in the repository.

6. The foundation selected space is listed.

7. The ideal memory site is updated for every particle.

8. Members dominated by the current populace are congregated at the depository, and the count of depository citizens rises.

9. Collected citizens in the depository are re-considered, and superior citizens are excluded.

10. If the count of citizens becomes greater than the highest range of the depository, then a segment of the populace will be excluded, and the list will be rebooted.

    In this case, when the last condition is not fulfilled, the algorithm goes back to the third step and the remaining steps are performed again, or the improvement method ends.

4.2. NSGA-II

NSGA-II algorithm steps are as follows [50, 54, 60]:

1. Set NSGA-II parameters.

   The most important parameters used are initial population size (N), composition (PC), mutation (PM), retention (PR), convergence (PCN), selection type, type of combination, and mutation operators.

2. It randomly initializes the population.

3. Calculates the primary function values of the target population for each chromosome.

4. Depending on the amount of PS, chromosome pairs are selected as parents. The parent selection process is performed using the stored values of the evaluation function.

5. Depending on the PC each pair of parents combines to produce one or two child chromosomes.

6. Each child's chromosome mutates according to the amount of PM.

7. Given the PR, several offspring are selected for replacement in the new generation, and the next generation of chromosomes from the previous generation is selected according to the rule of dominance as follows, thereafter the new generation is replaced by the previous generation in the program.

   Domination rule: x_1 (result 1) is superior than x_2 (result 2) if: (minimizing problem)

   a. All the objective functions are $f_i(x_1) \leqslant f_i(x_2)$ ranging between 1 to i.

   b. At least one objective function is $_i$ $(x_1) < f_i(x_2)$ ranging between 1 to i.

8. The case of algorithm stop, termination, and chromosomal convergence with optimal response was studied. If the stopping condition is not met, then resume running the algorithm from step 5. Otherwise, the best current generation chromosome will be selected as the final response and the algorithm terminates.

4.3. MCS

The MCS method is a calculation analysis which creates numerous stochastic situations. In fact, it uses random cases to compute the solution. This process is utilized to reproduce situations with higher levels of unreliability and requires more precise results [19].

The MCS technique creates numerous random data and improves predictions for the convergence problem.

In this research, because of the irregularities in the behavior of the EV, several scenarios are considered to determine entry and exit times and SOC at the entry to critically investigate the EV's random behavior. In addition, the uncertainty in entry and exit times and SOC at the entry of the EV is planned to utilize MCS, and a flowchart is shown in Figure 2.

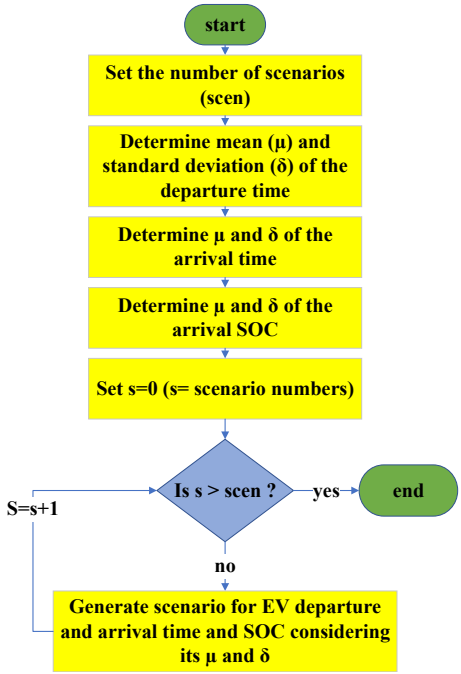

Figure 2: Flowchart of the MCS

4.4. Taguchi method

The design experimental design is the plan of the work that aims to illustrate a variety of factors under conditions which reflects the variation.

In this paper, the Taguchi method was used, which uses a set of tables called orthogonal arrays to design and perform experiments according to certain rules. Orthogonal arrays allow examination of the main and interaction effects with the least number of experiments [61, 62].

In fact, in Taguchi, scenarios are determined by orthogonal arrays. An orthogonal array is a matrix represented by $L_H(B^F)$. In Table 2, H and F represent the number of rows and columns of the matrix, respectively, while B represents the number of levels of the matrix elements (uncertainty variables). Table 2 shows the number of levels of the variables. Factor F represents the maximum number of factors (uncertainty variables) examined by the array [63].

In this research, the uncertainty in solar irradiance, wind speed, and load was

modeled using the Taguchi method, meaning that there is 3 uncertainty variables. Therefore, the orthogonal matrix must have 3 columns (i.e., F = 3). The first to third uncertainty variables in Taguchi calculations are assigned to the first to third columns. Hence, the Taguchi matrix table L9 is used, which is given in Table 3, and its flowchart is shown in Figure 3.

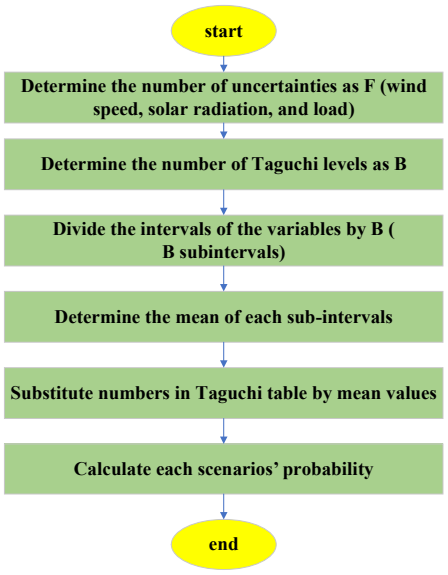

Figure 3: Flowchart of the MCS

Table 2: Number of levels w.r.t. factors

Level	**Factor**		
	F1	F2	F3
1	Low	Low	Low
2	Average	Average	Average
3	High	High	High

Table 3: Orthogonal array of L_9

N^a of tests	**According to Taguchi table** L_9		
	F1	F2	F3
1	1	1	1
2	1	2	2
3	1	3	3
4	2	1	2
5	2	2	3
6	2	3	1
7	3	1	3
8	3	2	1
9	3	3	2

5. Result and discussion

The MOPSO and NSGA-II algorithms are used to design the different configurations of energy sources considered for a typical household, listed in five different cases. In fact, the pseudo-codes of which are shown in Algorithm 1. For this research, the decision variables consist of units of WT, PV, DG, battery, FC, EL, and HT components, and the grid decision variables are hourly powered. Moreover, the search space for all variables except for the battery is between 0 and 100 kW, and 0 to 100 kWh in the case of the battery. The specifications of the MOPSO program contain w = 0.8, N = 100, $c_1 = 2$, $c_2 = 2$, $\beta = 2$, and TR = 30, where TR refers to total repetitions, N is equal to total particles, w is the weight of inertia, and as per a general rule, w is below 1, and c_1, c_2, and β are the constants of the algorithm. In addition, the specifications of the NSGA-II program contain N = 100, PC = 0.1, PM = 0.02, PR = 100, and PCN = 0.9, where N is the population, PC is the composition probability, PM is the mutation probability, PR is the retention probability, and PCN is the convergence probability, respectively.

CS1

Data: the required parameters (P^L, wind speed, solar radiation, $SOC^{b,max}$ and $SOC^{b,min}$, MOPSO and NSGA-II parameters, and economic data related to PV, WT, battery, and DG)

Result: N^{PV}, N^{WT}, N^b, and N^{DG}

initialization;

$$P_t^S = P_t^{PV} + P_t^{WT} + P_t^{DG} + P_t^b - P_t^L; \tag{65}$$

t=0;

t= time (hour)

while $t < 24$ **do**

  if $P^{PV} + P^{WT}$ *can meet the* P^L **then**

    if $SOC^b < SOC^{b,max}$ **then**

      Charge Battery with excess power;

    end

  else

    Meet the P^L with P^{DG};

    Turn on the DG;

    Calculate CO_2;

  end

  Calculate LCC, LPSP, and CO_2;

  t=24;

end

CS2

Data: the required parameters (P^L, wind speed, solar radiation, $SOC^{b,max}$ and $SOC^{b,min}$, MOPSO and NSGA-II parameters, and economic data related to PV, WT, battery, FC, EL, and HT)

Result: N^{PV}, N^{WT}, N^b, N^{FC}, N^{EL}, and N^{HT}

initialization;

$$P_t^S = P_t^{PV} + P_t^{WT} + P_t^{FC} + P_t^b - P_t^L; \tag{66}$$

t=0;

Algorithm 1: PSEUDO-CODE FOR CS1, CS2, CS3, CS4, AND CS5

while $t < 24$ **do**

  if $P^{PV} + P^{WT}$ *can meet the* P^{L} **then**

    if $SOC^{b} < SOC^{b,max}$ **then**

      Charge Battery with excess power;

      if *excess power after charging battery remains* **then**

        Inject power into EL;

        Store hydrogen into HT;

      end

    else

      Inject power into EL;

      Store hydrogen into HT;

    end

  else

    if *battery is not empty* **then**

      Discharge the battery

    else if *the battery is empty & the HT is not empty* **then**

      Inject hydrogen from HT into FC;

      Meet the P^{L} with the P^{FC};

  end

  Calculate LCC and LPSP;

  t=24;

end

CS3

Data: the required parameters (P^{L}, wind speed, solar radiation, $SOC^{b,max}$ and $SOC^{b,min}$, MOPSO and NSGA-II parameters, and economic data related to PV, WT, battery, and grid)

Result: N^{PV}, N^{WT}, N^{b} and P^{grid}

initialization;

$$P_t^S = P_t^{PV} + P_t^{WT} + P_t^{grid} + P_t^b - P_t^L; \tag{67}$$

t=0;

5.1. Information accumulation

✓ load/ Wind speed/ Solar irradiance

Required load data was obtained from the Kurdistan Electricity Company, and the values of solar irradiance and wind speed obtained from [64] during the year are shown in Figure 4.

✓ Taguchi results

Figure 5 shows data of load consumption, solar irradiance, and wind speed at three different levels, obtained using the Taguchi method.

✓ Costs information

The prices to install, renew, and run per kW of WT, PV, DG, FC, EL, and HT and per kWh of battery are shown in Table 4, and also, the price to buy grid power within 24 hours is shown in Table 5. In addition, the price demand elasticity is considered as listed in Table 6.

while $t < 24$ **do**

  if $P^{PV} + P^{WT}$ *can meet the* P^{L} **then**

    if $SOC^{b} < SOC^{b,max}$ **then**

      Charge Battery with excess power;

      if *excess power after charging battery remains* **then**

        Sell the excess power to the grid;

      end

    else

      Sell the extra power to the grid;

    end

  else

    if *battery is not empty* **then**

      Discharge battery to meet the load

    else if *the battery is empty* **then**

      Buy deficit power from the grid;

  end

  Calculate LCC and LPSP and CO_2;

  t=24;

end

CS4

Data: the required parameters ($P^{L,new}$, wind speed, solar radiation, $SOC^{b,max}$, $SOC^{b,min}$, MOPSO and NSGA-II parameters, and economic data related to PV, WT, battery, and grid)

Result: N^{PV}, N^{WT}, N^{b} and P^{grid}

initialization;

$$P_t^S = P_t^{PV} + P_t^{WT} + P_t^{grid} + P_t^b - P_t^{L,new}; \tag{68}$$

t=0;

while $t < 24$ **do**

  if P^{PV}+ P^{WT} *can meet the* P^{L} **then**

    if $SOC^{b} < SOC^{b,max}$ **then**

      Charge Battery with excess power;

      if *excess power after charging battery remains* **then**

        Sell the excess power to the grid;

      end

    else

    end

  else

    Buy deficit power from grid **if** *DRP price is low & the battery is not full* **then**

      Charge the battery with grids power

    end

  end

  Calculate LCC and LPSP and CO_2;

  t=24;

end

CS5

Data: the required parameters (P^{L}, wind speed, solar radiation, $SOC^{b,max}$, $SOC^{b,min}$, $SOC^{EV,max}$, $SOC^{EV,min}$, MOPSO and NSGA-II parameters, and economic data related to PV, WT, and battery)

Result: N^{PV}, N^{WT}, and N^{b}

initialization;

$$P_t^S = P_t^{PV} + P_t^{WT} + P_t^{EV} + P_t^b - P_t^L; \tag{69}$$

t=0;

while $t < 24$ **do**

  if $P^{PV} + P^{WT}$ *can meet the* P^{L} **then**

    if $SOC^{b} < SOC^{b,max}$ **then**

      Charge Battery with excess power;

      if *excess power after charging battery remain & EV is available &* $SOC^{EV} < SOC^{EV,max}$ **then**

        Charge the EV;

      end

    else if $SOC^{EV} > SOC^{EV,max}$ **then**

      Discharge the EV to meet the P^{L};

  else

  end

  Calculate LCC and LPSP;

  t=24;

end

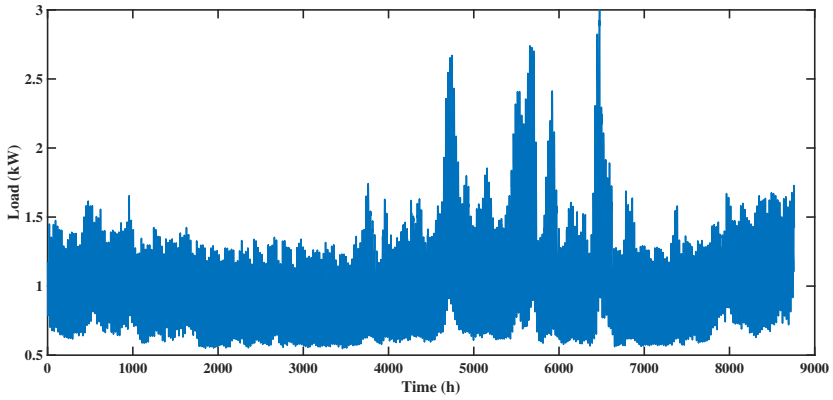

(a) Load consumption

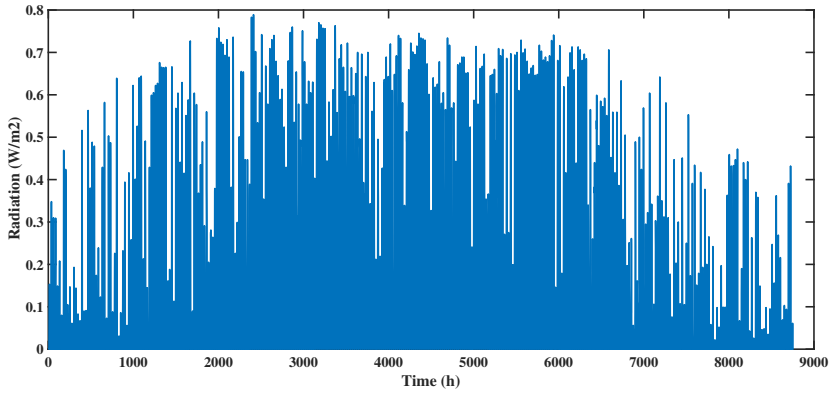

(b) solar irradiance

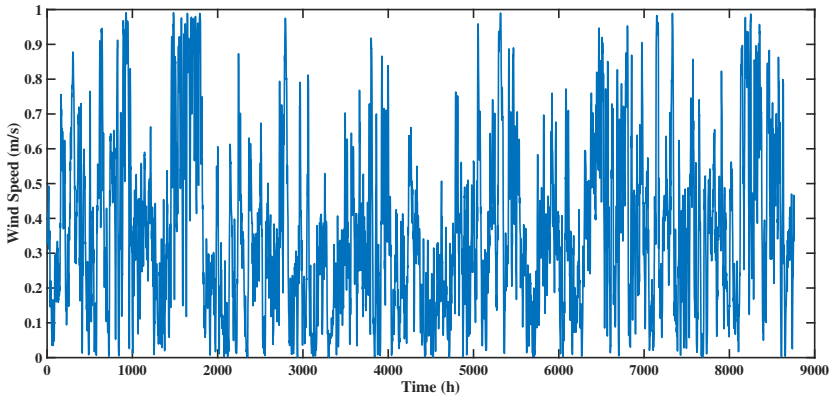

(c) wind speed

Figure 4: (a) Load consumption, (b) solar irradiance, and (c) wind speed

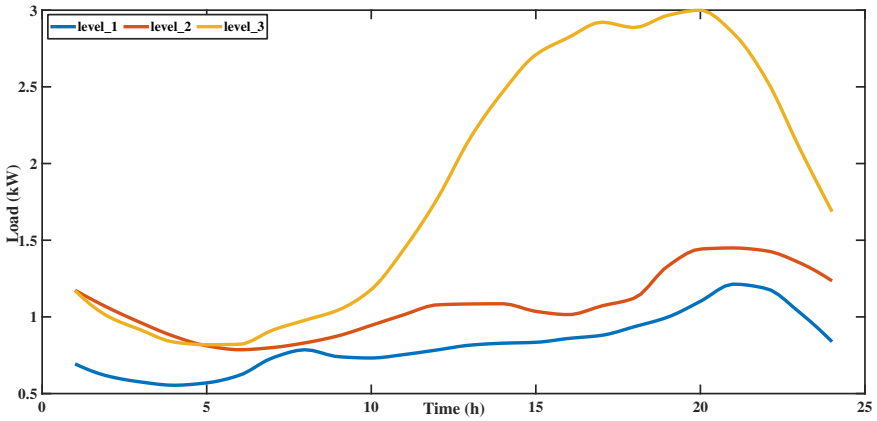

(a) Load consumption

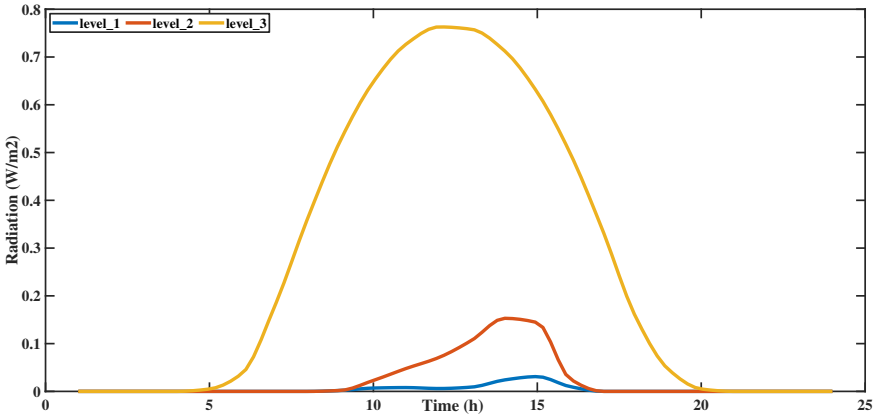

(b) solar irradiance

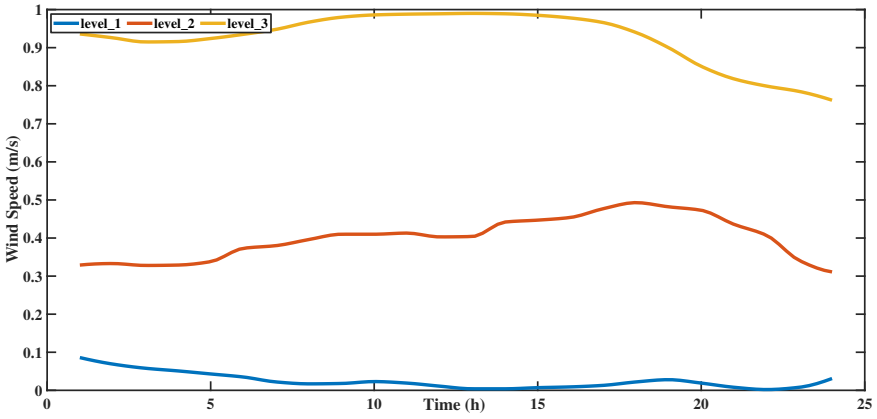

(c) wind speed

Figure 5: Results from the Taguchi method at three different levels in 24 hours for (a) load consumption, (b) solar irradiance, and (c) wind speed

Table 4: characteristics of the devices

Economical parameters	
Project lifetime	20 years
PV parameters	
PV lifespan	20 years
IC^{PV}	2000 ($)
MC^{PV}	33 ($)
WT parameters	
WT lifespan	20 years
IC^{WT}	3200 ($)
MC^{WT}	100 ($)
Battery parameters	
Battery lifespan	5 years
IC^{b}	100 ($)
MC^{b}	5 ($)
RC^{b}	100 ($)
DG parameters	
DG lifespan	15,000 (h)
IC^{DG}	550 ($)
p^{f}	0.45 ($/L)
FC parameters	
FC lifespan	5 years
IC^{FC}	6,000 ($)
MC^{FC}	120 ($)
RC^{FC}	4,000 ($)
EL parameters	
EL lifespan	15 years
IC^{EL}	4,000 ($)
MC^{EL}	20 ($)
RC^{EL}	3,000 ($)
HT parameters	
HT lifespan	20 years
IC^{HT}	3,960 ($)
MC^{HT}	79,2 ($)

Table 5: The cost of purchasing power from the grid in 24 hours [65]

Time (hour)	1	2	3	4	5	6
$/kWh	0.234	0.187	0.146	0.13	0.13	0.203
Time (hour)	7	8	9	10	11	12
$/kWh	0.234	0.379	1.505	4.005	4.005	4.005
Time (hour)	13	14	15	16	17	18
$/kWh	1.505	4.006	1.998	1.957	0.613	0.426
Time (hour)	19	20	21	22	23	24
$/kWh	0.348	0.426	1.183	0.54	0.306	0.265

Table 6: Characteristics of the elasticity [58]

	Peak	Off-peak	Low load
Peak	-0.01	0.016	0.012
Off-peak	0.016	-0.1	0.01
Low load	0.012	0.01	-0.1

✓ EV features

Table 7 provides the features of an EV and the time of entry and leaving is based on literature [19]. In addition, the state of charge at entry time of an EV follows the normal distribution function as represented in Figure 6. Nevertheless, at least one minimum value should be defined in the EV's SOC when leaving because the EV should have the charge to travel from home to the charging station.

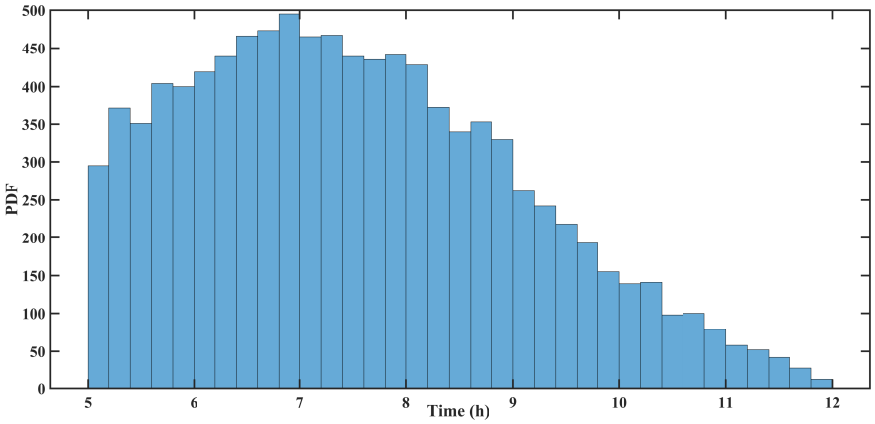

(a) leaving time

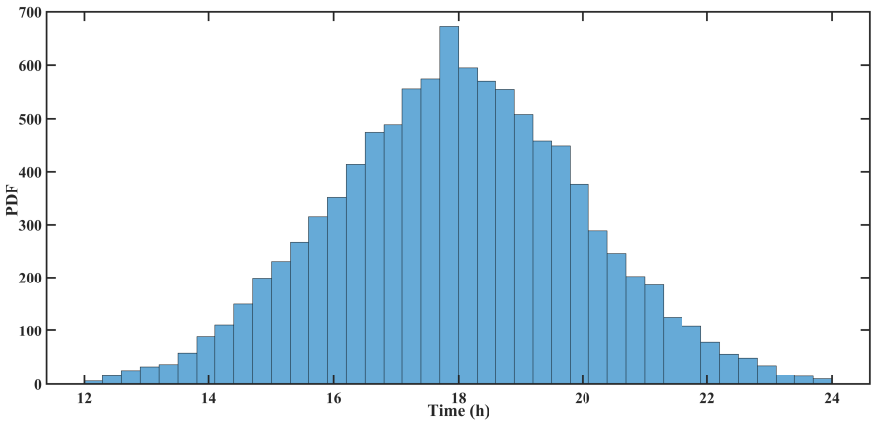

(b) entry time

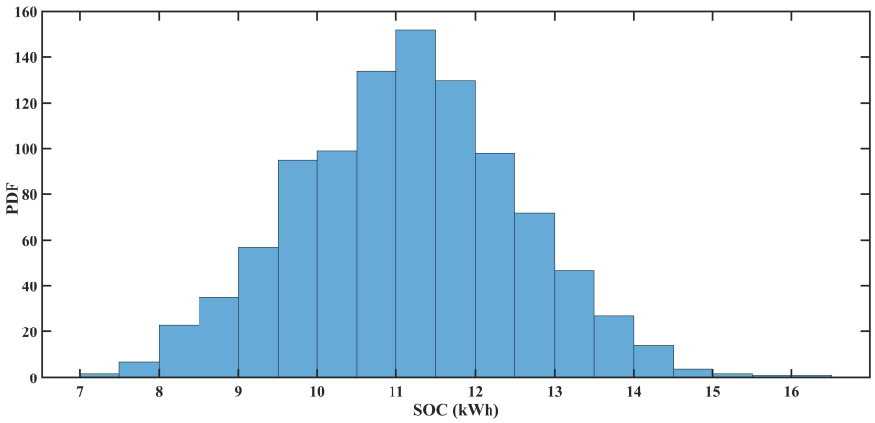

(c) SOC at arrival

Figure 6: Normal distribution functions of the EV (a) leaving time, (b) entry time, and (c) SOC at arrival.

Table 7: Input constraints for EV

EV constraints	
Cap^{EV}	14 (kWh)
SOC^{EV}_{max}	95 (%)
SOC^{EV}_{min}	10 (%)
EV entry time constraints	
μ^{EV}_{a}	18
σ^{EV}_{a}	2
$12 \leqslant T^{EV}_{arrive} \leqslant 24$	
EV leaving time constraints	
μ^{EV}_{d}	7
σ^{EV}_{d}	2
$5 \leqslant T^{EV}_{dep} \leqslant 12$	
EV arrival SOC constraints	
$SOC^{EV}_{dep} \geqslant 0.2 \times 14$	
EV departure SOC constraints	
μ^{EV}_{a}	0.8×14
σ^{EV}_{a}	0.1×14

5.2. MOPSO results

5.2.1. CS1 (PV/ WT/ battery/ DG)

In this case, the energy required by the user for 20 years is obtained through the energy produced by the PV/ WT/ battery/ DG model. For the mentioned configuration, the optimal solutions gained from the MOPSO algorithm are also suitable in terms of LCC, LPSP, and CO_2, are shown in Figure 7. Among these solutions, the optimal point at zero LPSP is considered, where the configuration accomplishment of this arrangement is provided in Table 8, where 10 PV, WT, and battery units and 3 DG units are selected. Further, the behavior of PV, WT, battery, and DG components in this optimized solution is shown in Figure 8 for 24 hours.

Table 8: Configuration of one of the optimal points obtained from MOPSO algorithm at zero LPSP for CS1

LPSP (%)	PV (kW)	WT (kW)	battery (kWh)	DG (kW)	LCC ($)	co_2 (kg)
0	10	10	10	3	183,014.9	86,753.34

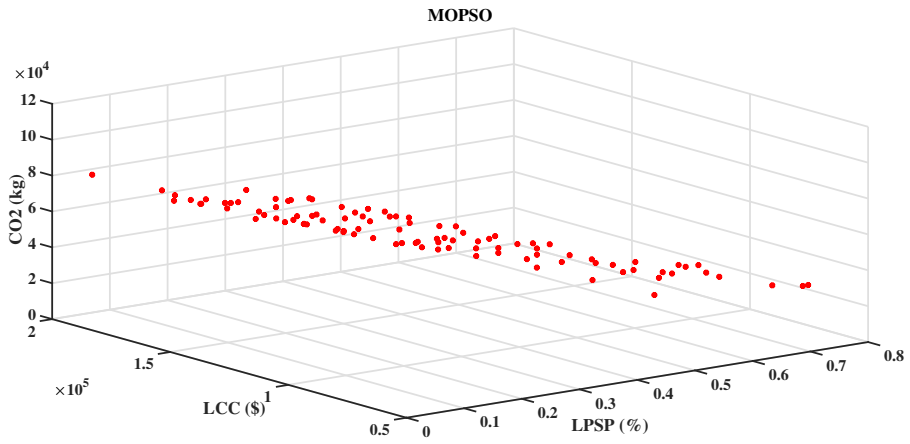

Figure 7: Three-dimensional Pareto surface for the CS1

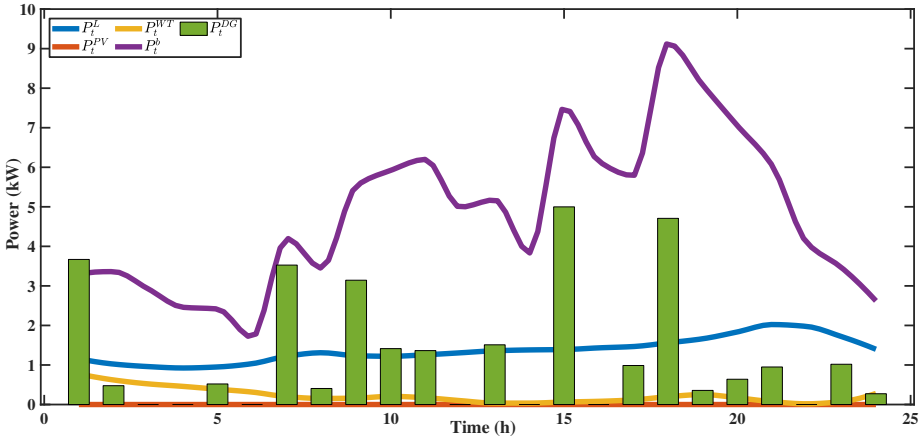

Figure 8: MOPSO simulation results for the CS1

5.2.2. CS2 (PV/ WT/ battery/ FC/ EL/ HT)

The system designed for this scenario is PV/ WT/ battery/ FC/ EL/ HT, which produces the energy required by the user for 20 years. For this configuration, the optimal solutions obtained from the MOPSO algorithm that are suitable with regard to price and security are shown in Figure 9 (in this scenario, the Pareto surface is two-dimensional, as none of the sources produce pollution). Among these solutions, the optimal point at zero LPSP is considered, and the configuration outcomes of this are demonstrated in Table 9, where selected components equipped with an equal number of 1 PV, 13 batteries, 2 FC, and 3 EL units. Moreover, no pollution is produced in this case, the cost is $ 306,937.4, which is much more than other systems. In addition, the behavior of each of the WT, PV, battery, and FC elements is shown in Figure 10 for 24 hours.

Table 9: Configuration of one of the optimal points obtained from MOPSO algorithm at zero LPSP for CS2

LPSP (%)	PV (kW)	WT (kW)	battery (kWh)	FC (kW)	EL (kW)	HT (kW)	LCC ($)	co_2 (kg)
0	1	0	13	2	3	0	306,937.4	0

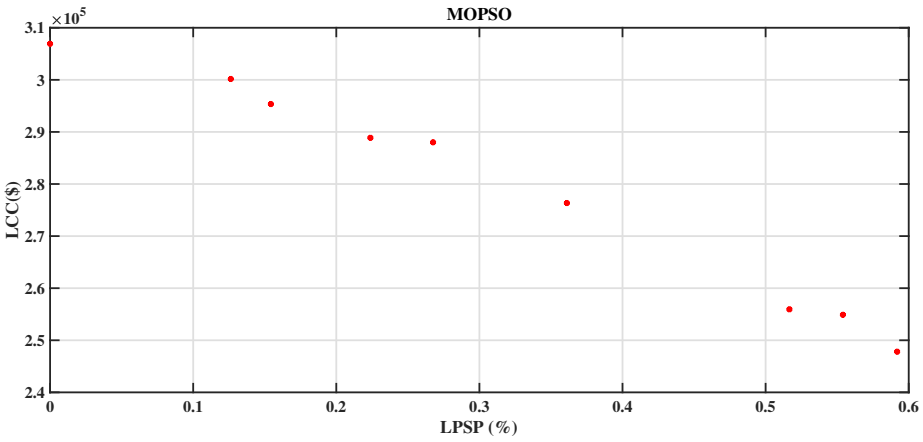

Figure 9: Two-dimensional Pareto surface for the CS2

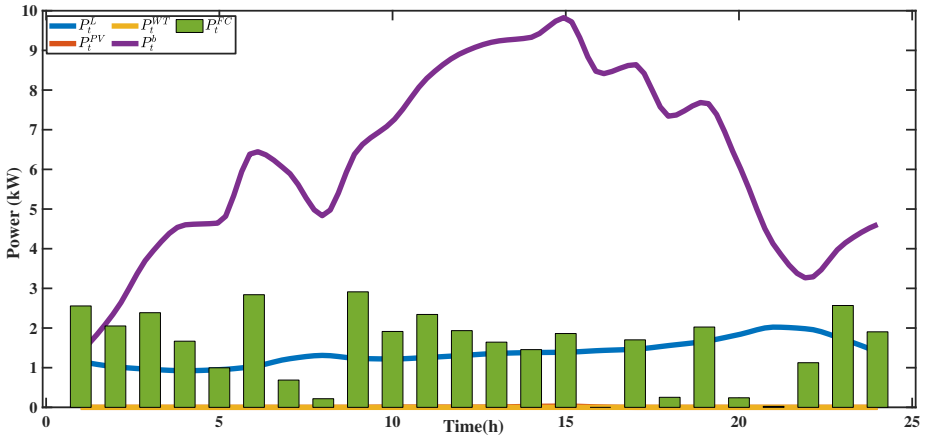

Figure 10: MOPSO simulation results for the CS2

5.2.3. CS3 (PV/ WT/ battery/ grid-connected)

In this case, the energy the user needs for 20 years is obtained through the energy produced by the PV/ WT/ battery/ grid-connected system. For this configuration, the optimal solutions obtained from the MOPSO algorithm, which are also suitable in terms of LCC, LPSP, and CO_2, are shown in Figure 11. Among these solutions, the optimal point at zero LPSP is considered, and the configuration performance of this system is given in Table 10, where 1 PV unit and 10 battery units are selected. Further, the behavior of each PV, WT, and battery component, along with the power given and taken from the grid, is shown for this solution in Figure 12 for 24 hours, and, as is known, used in all hours except 6, 9, 14, 17, and 20, which gave power of 0.46 kW, 0.59 kW, 0.85 kW, 2.17 kW, and 0.69 kW to the grid, respectively, and received power from the grid.

Table 10: Configuration of one of the optimal points obtained by the MOPSO algorithm at zero LPSP for CS3

LPSP (%)	PV (kW)	WT (kW)	battery (kWh)	LCC ($)	co_2
0	1	0	10	218,505.8	470,924.1

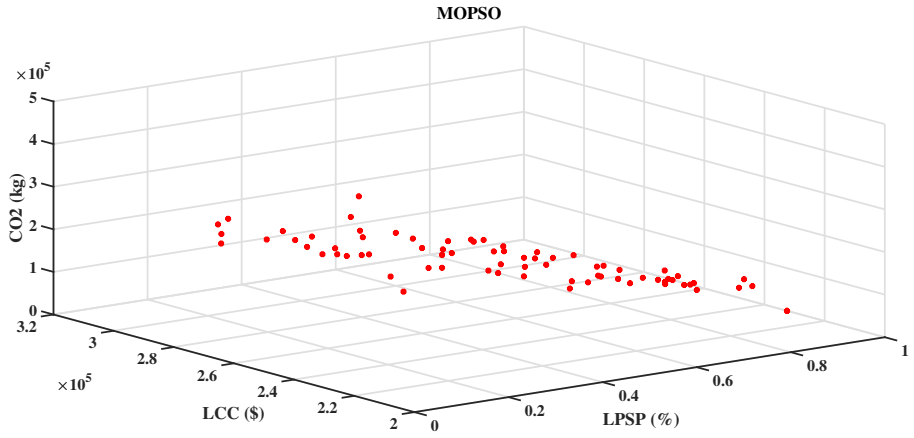

Figure 11: Three-dimensional Pareto surface for the CS3

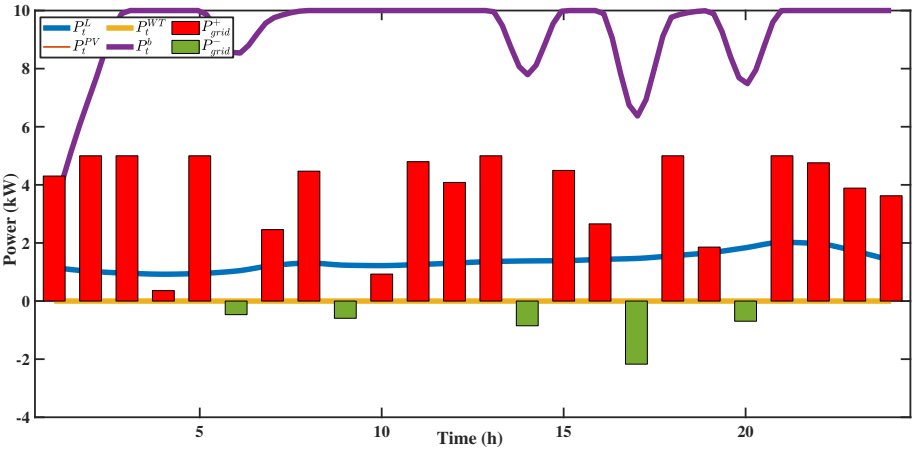

Figure 12: MOPSO simulation results for the CS3

5.2.4. CS4 (PV/ WT/ battery/ grid-connected with DRP)

In this case, the PV/ WT/ battery/ grid-connected with DRP is designed to provide the energy required by the user for 20 years. In fact, the demand response program based on TOU price is considered. According to Figure 13, the demand is increased as costs decrease during off-peak hours, and the demand is decreased as costs increase during off-peak hours. It is clear that considering the DRP has had a significant impact on reducing costs and pollution. For this configuration, the opti-

mal solutions obtained from the MOPSO algorithm, which are also suitable in terms of LCC, LPSP, and CO_2, as shown in Figure 14. Among these solutions, the optimal point at zero LPSP is considered, where the configuration performance of this system is given in Table 11, where 2 PV and 10 battery units are selected. Further, the behavior of each component of PV, WT, and battery, as well as the power given and taken from the grid, is shown in Figure 15 for 24 hours, and, as it is known, used in all hours except 7, 10, 19, and 20, which gave power of 2.79 kW, 3.37 kW, 3 kW, and 1.15 kW to the grid, respectively, and received power from the grid.

Table 11: Configuration of one of the optimal points obtained from the MOPSO algorithm at zero LPSP for CS4

LPSP (%)	PV (kW)	WT (kW)	battery (kWh)	LCC ($)	co_2
0	2	0	10	20,328.2	402,545

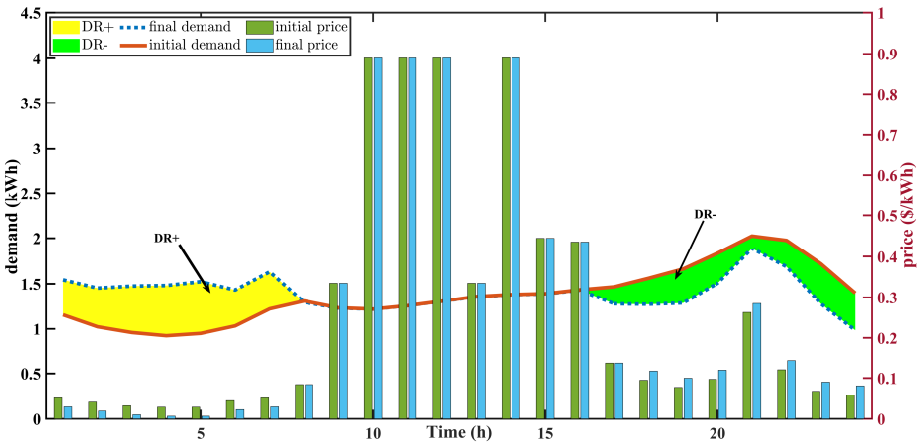

Figure 13: Implementation of a DRP based on TOU price in CS4

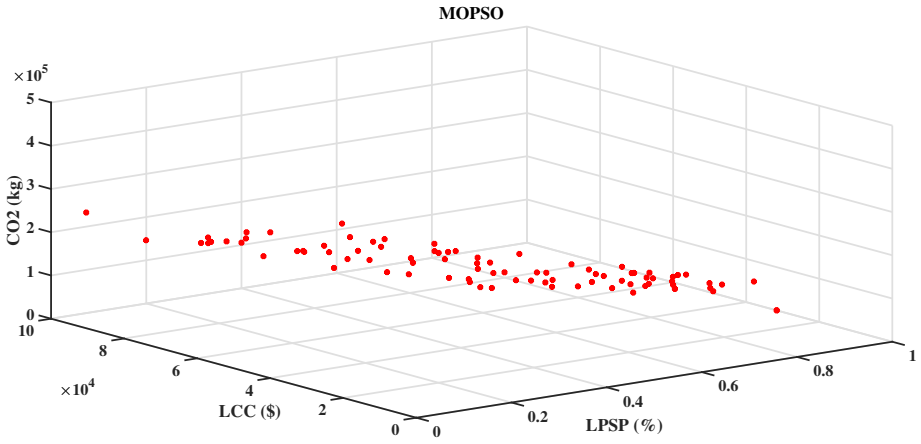

Figure 14: Three-dimensional Pareto surface for the CS4

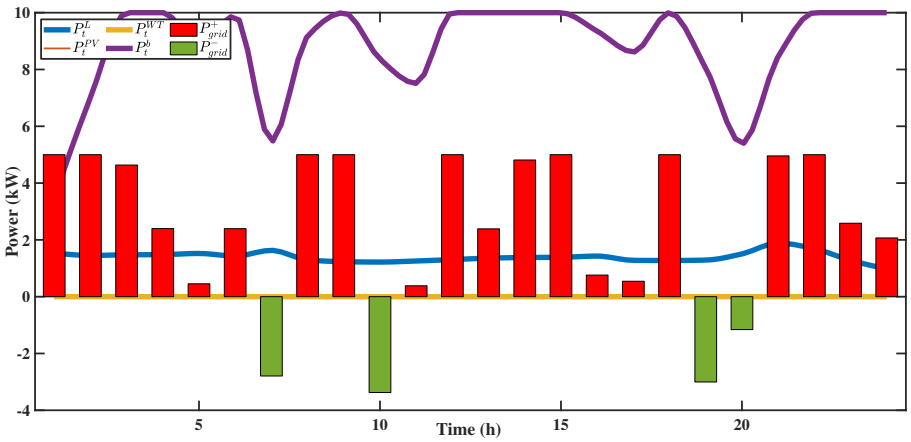

Figure 15: MOPSO simulation results for the CS4

5.2.5. CS5 (PV/ WT/ battery/ EV)

For this study, the PV/ WT/ battery/ EV arrangement was designed to provide the energy required by the user for 20 years, and the EV's irregular conduct was also modeled using Monte Carlo simulations. It can be observed that EV's entry and leaving times and SOC at arrival relate to the function of normal distribution, which means leaving time ranges between 5 and 12, and 12 to 24 for the entry time. The SOC at the entry time ranges between 6 kWh and 13.3 kWh, however the SOC at

leaving is restricted and above 0.2×14. For this configuration, the appropriate and optimal solutions obtained from the MOPSO algorithm regarding price and security are shown in Figure 16 (in this study, the Pareto surface is two-dimensional, as none of the sources produces emissions). Among these solutions, the optimal point at zero LPSP is considered, and the configuration performance of this system is given in Table 12, where the sources required for power supply are 63 WT units and 12 battery units. As shown in this case, the pollution is zero. Further, the behavior of each component for this answer is shown in Figure 17, and as it is clear at this optimal point, the behavior of the EV is such that at 7 o'clock with power, 3.087 kW leaves the house, and at approximately 18 hours with power, 10.95 kW returns home. Therefore, it is clear that the EV started to discharge as soon as it entered the house because the production capacity of other sources was less than the desired load at that time.

Table 12: Configuration of one of the optimal points obtained from the MOPSO algorithm at zero LPSP for CS5

LPSP (%)	PV (kW)	WT (kW)	battery (kWh)	LCC ($)	co_2
0	0	63	12	334,800	0

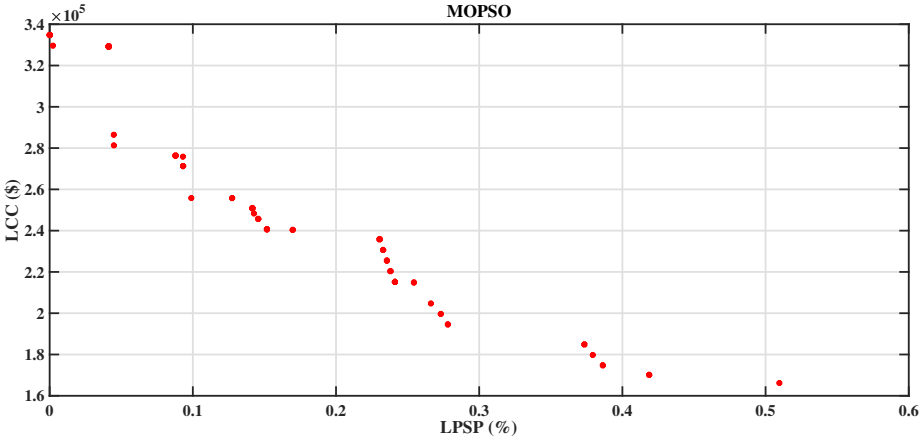

Figure 16: Two-dimensional Pareto surface for the CS5

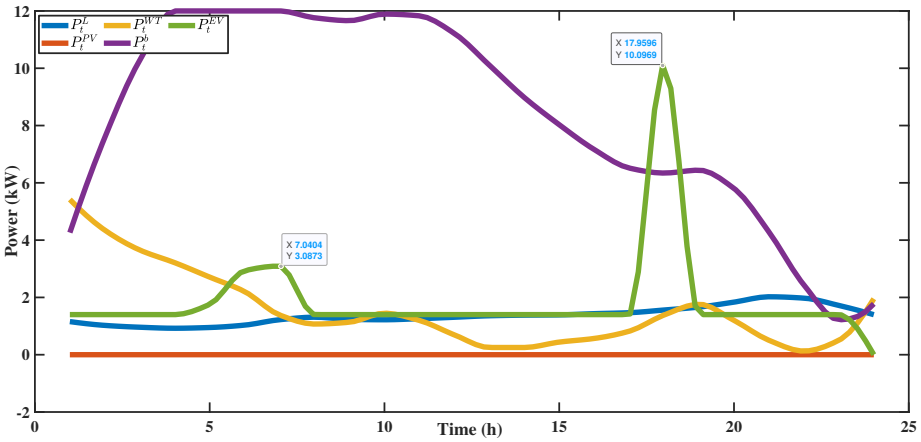

Figure 17: MOPSO simulation results for the CS5

5.3. NSGA-II results

5.3.1. CS1 (PV/ WT/ battery/ DG)

For this study, the energy required by the user for 20 years is obtained through the energy produced by the PV/ WT/ battery/ DG model. For this configuration, the optimal solutions obtained from the NSGA-II algorithm, which are also suitable in terms of LCC, LPSP, and CO_2, are shown in Figure 18. Among these solutions, the optimal point at zero LPSP is considered, where the configuration performance of this system is given in Table 13, where PV, WT, five battery units, and two DG units are selected. Moreover, the behavior of the PV, WT, battery, and DG components in this optimal solution is shown in Figure 19 for 24 hours.

Table 13: Configuration of one of the optimal points obtained from NSGA-II algorithm at zero LPSP for CS1

LPSP (%)	PV (kW)	WT (kW)	battery (kWh)	DG (kW)	LCC ($)	co_2
0	1	1	5	2	118,391.9	95,246.68

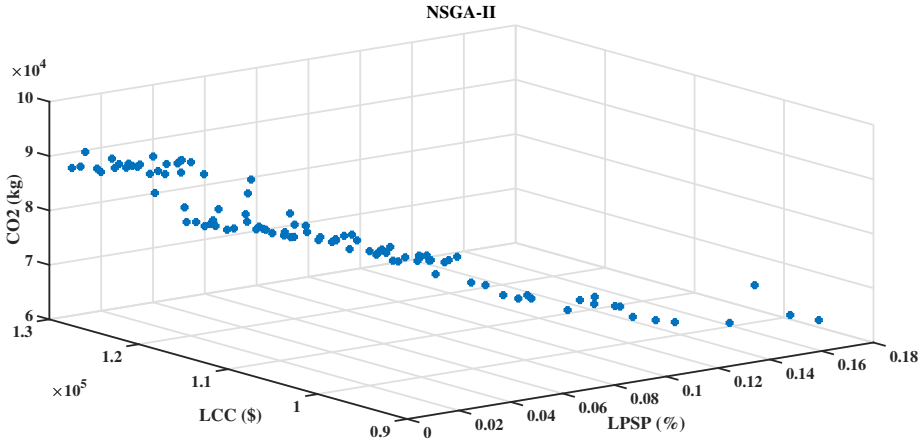

Figure 18: Three-dimensional Pareto surface for the CS1

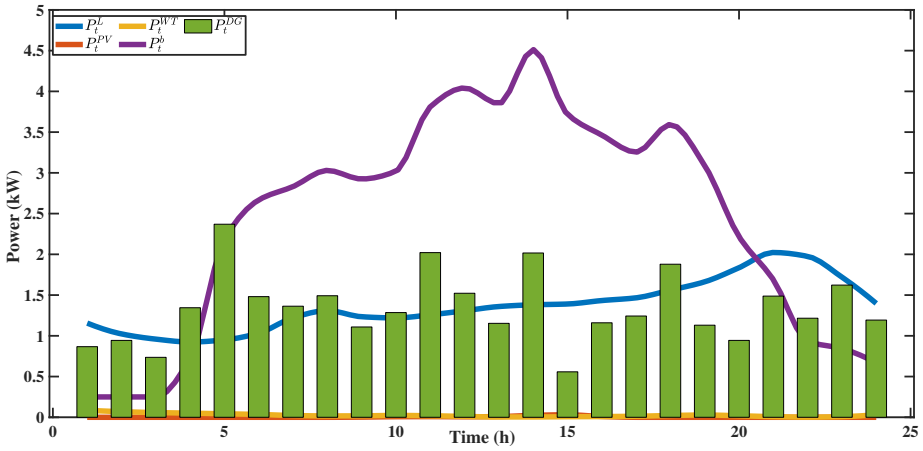

Figure 19: NSGA-II simulation results for the CS1

5.3.2. CS2 (PV/ WT/ battery/ FC/ EL/ HT)

The system designed in this case is PV/ WT/ battery/ FC/ EL/ HT, which produces the energy required by the user for 20 years. For this configuration, the optimal solutions obtained from the NSGA-II algorithm, which are suitable for price and security, are shown in Figure 20 (in this study, the Pareto surface is two-dimensional, as none of the sources produce pollution). Among these solutions, the optimal point of zero LPSP is considered, and the configuration performance of this system is given

in Table 14, where the selected components are equal to 9 PV units, 1 WT unit, 17 batteries, 2 FC, and 3 EL units. As it can be seen, no pollution is produced in this case, but the cost is $ 371,869.7, which is much more than other systems. Moreover, the behavior of the PV, WT, battery, and FC components is shown in Figure 21 for 24 hours.

Table 14: Configuration of one of the optimal points obtained from the NSGA-II algorithm at zero LPSP for CS2

LPSP (%)	PV (kW)	WT (kW)	battery (kWh)	FC (kW)	EL (kW)	HT (kW)	LCC ($)	co_2
0	9	1	17	2	2	2	371,869.7	907,24.8

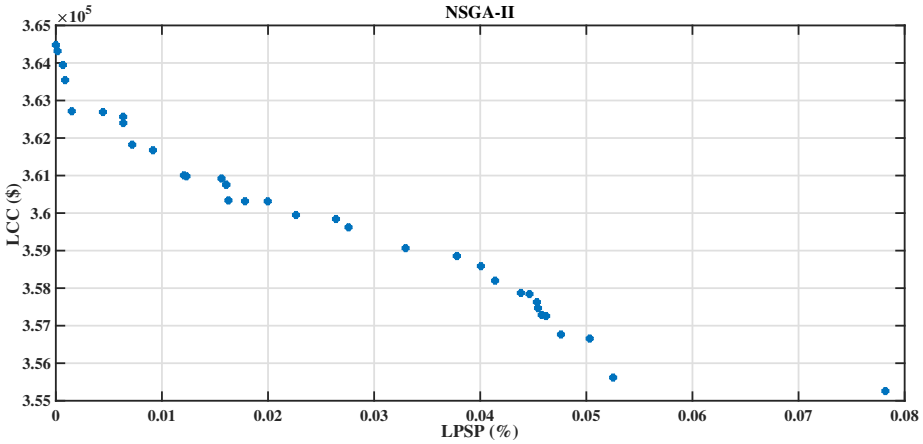

Figure 20: Two-dimensional Pareto surface for the CS2

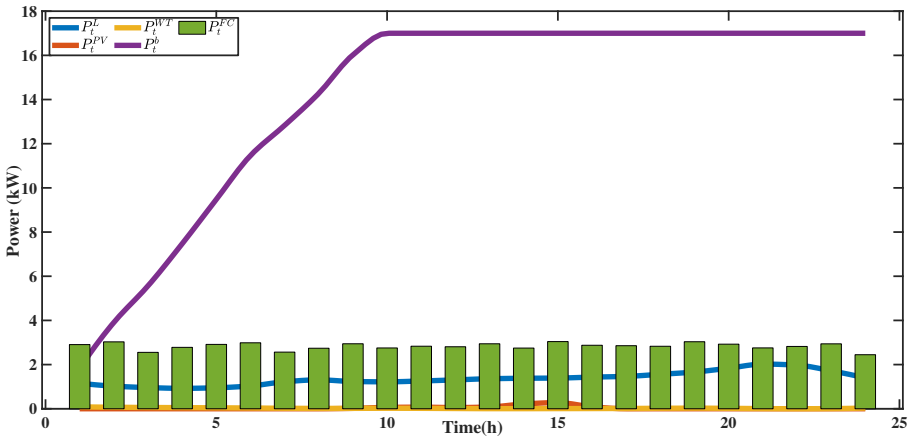

Figure 21: NSGA-II simulation results for the CS2

5.3.3. CS3 (PV/ WT/ battery/ grid-connected)

In this case, the energy required by the user for 20 years is obtained through the energy produced by the PV/ WT/ battery/ grid-connected system. For this configuration, the optimal solutions gained from the NSGA-II algorithm, which are suitable in terms of LCC, LPSP, and CO_2, are shown in Figure 22. Among these solutions, the optimum point of zero LPSP is considered, and the configuration performance of this system is given in Table 15, where 1 PV unit and 7 battery units are selected. Further, the behavior of each component of PV, WT, and battery, as well as the power given and taken from the grid, is presented in Figure 23 for 24 hours. According to the Figure, it was in all hours except 9 and 16, which gave 1.34 kW and 0.07 kW to the grid, respectively, and received power from the grid.

Table 15: Configuration of one of the optimal points obtained from the NSGA-II algorithm at zero LPSP for CS3

LPSP (%)	PV (kW)	WT (kW)	battery (kWh)	LCC ($)	co_2
0	1	0	7	215,627.1	237,746.5

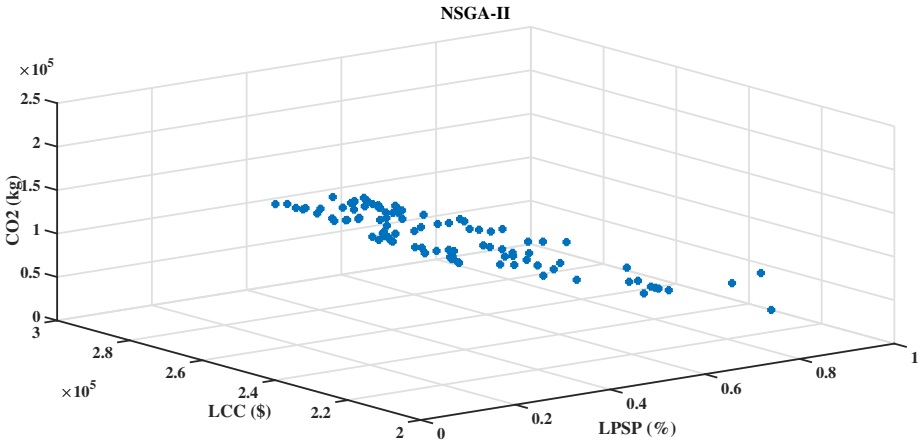

Figure 22: Three-dimensional Pareto surface for the CS3

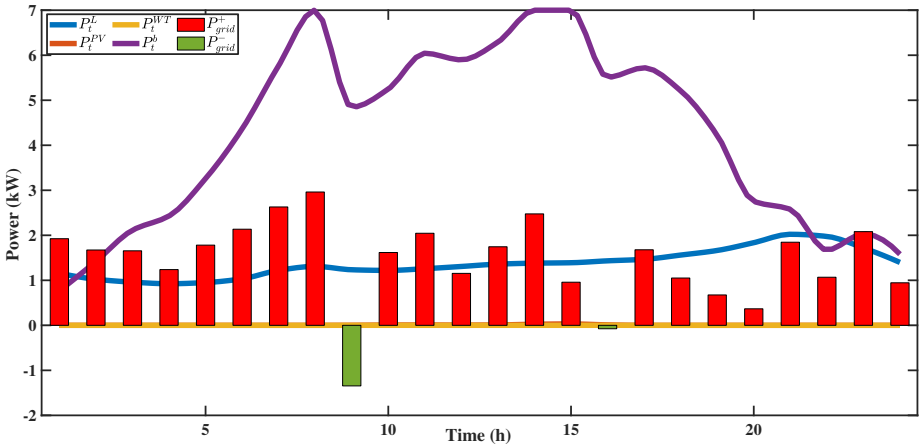

Figure 23: NSGA-II simulation results for the CS3

5.3.4. CS4 (PV/ WT/ battery/ grid-connected with DRP)

In this case, the PV/ WT/ battery/ grid-connected with DRP is designed to provide the energy required by the user for 20 years. In fact, in this case, the DRP based on the TOU price is considered. According to Figure 13, the demand increased as costs decreased during off-peak hours and decreased as costs increased during off-peak hours. However, the DRP could impact significantly on reducing costs and pollution. For this configuration, the optimal solutions obtained from the NSGA-II

algorithm, which are also suitable in terms of LCC, LPSP, and CO_2, are shown in Figure 24. Among these solutions, the optimal point of zero LPSP is considered, and the configuration performance of this system is given in Table 16, where 1 PV unit and 6 battery units are selected. In addition, the behavior of each component of PV, WT, and battery, as well as the power given and taken from the grid, is represented in Figure 25, for 24 hours. With respect to the Figure, it was used in all hours except 18, 20, and 24, which gave power of 0.28 kW, 0.07 kW, and 0.14 kW to the grid, respectively, and received power from the grid.

Table 16: Configuration of one of the optimal points obtained from the NSGA-II algorithm at zero LPSP for CS4

LPSP (%)	PV (kW)	WT (kW)	battery (kWh)	LCC ($)	co_2
0	1	0	6	15,933.43	241,004

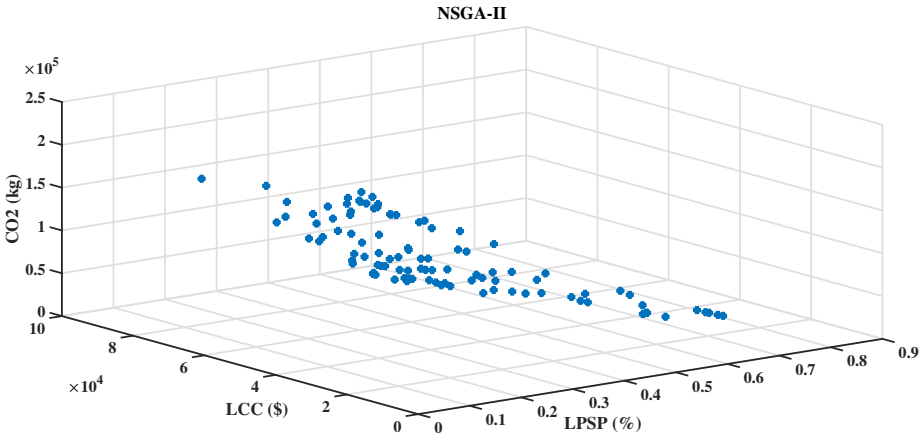

Figure 24: Three-dimensional Pareto surface for the CS4

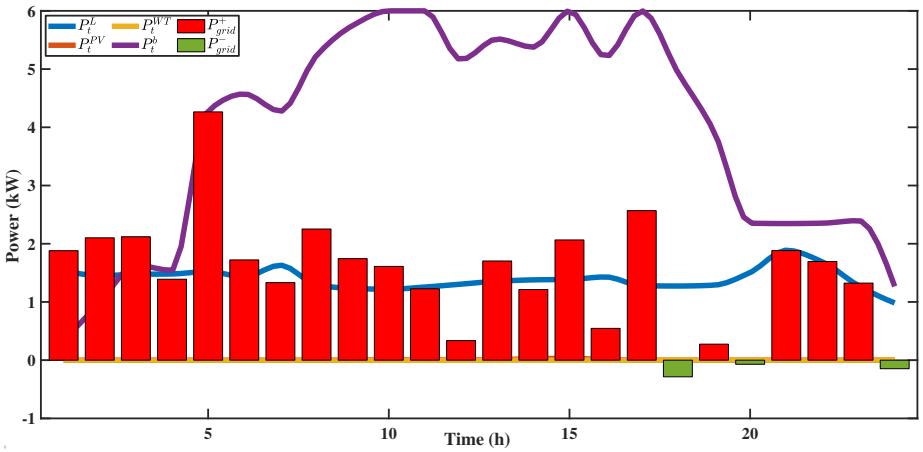

Figure 25: NSGA-II simulation results for the CS4

5.3.5. CS5 (PV/ WT/ battery/ EV)

In this case, the PV/ WT/ battery/ EV model was designed to provide the energy required by the user for 20 years, and the EV's random functioning was modeled by Monte Carlo simulations. It can be observed that the EV's entry and leaving times, and its SOC at entry, follow the normal distribution function, which means that the EV's time of leaving is between 5 and 12, and the time of entry is between 12 and 24. Further, the SOC at the time of entry also changes in a range of 6 kWh to 13.3 kWh. However, SOC at the time of leaving must be above 0.2×14. For this configuration, the optimal solutions obtained from the NSGA-II algorithm that are suitable both in regards to price and security are shown in Figure 26 (in this study, the Pareto surface is two-dimensional, as none of these sources produce emissions). Among these solutions, the optimum point of zero LPSP is considered, and Table 17 shows the configuration achievements, where the sources required for power supply are 62 WT units and 12 battery units. Moreover, it is clear that the pollution is zero. Additionally, the behavior of each component for this answer is shown in Figure 27, and at this optimal point, the behavior of the EV is at 6 o'clock with a power of 3.345 kWh, leaves the house, and returns home at approximately 17 with a power of 10.307 kWh. Further, the EV started to discharge as soon as it entered the house because the production capacity of other sources was less than the desired load at

that time.

Table 17: Configuration of one of the optimal points obtained from the NSGA-II algorithm at zero LPSP for CS5

LPSP (%)	PV (kW)	WT (kW)	battery (kWh)	LCC ($)	co_2
0	0	62	12	330,980.4	0

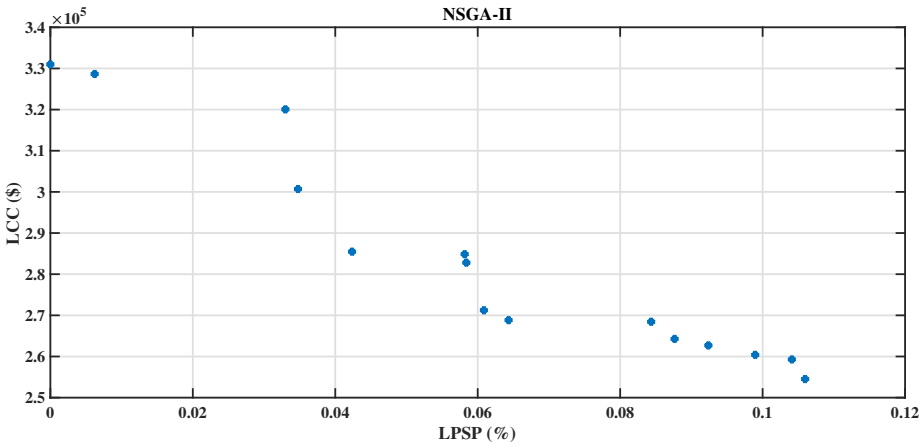

Figure 26: Two-dimensional Pareto surface for the CS5

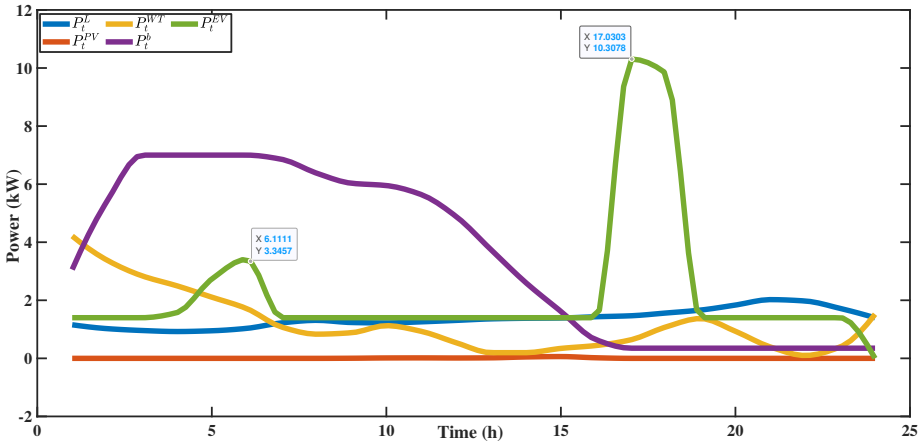

Figure 27: NSGA-II simulation results for the CS5

5.4. Comparison of results

In this section, the intended target is to compare LCC, LPSP, and CO_2 in different five case studies, which are calculated using two algorithms, MOPSO and NSGA-II. In Figure 28(a), the LCC was compared and examined in all five cases using both algorithms. Further, the most optimal LCC relates to CS4 in both algorithms.

In Figure 28(b), the LPSP was compared and examined in all five cases calculated using both algorithms. In fact, CS1 is designed by the NSGA-II algorithm, is the best system in terms of LPSP. It can also be observed that in all five systems, the NSGA-II algorithm provides us with more efficient solutions than MOPSO. Moreover, in Figure 28(c), CO_2 was compared and investigated in five distinct scenarios calculated using both algorithms. Additionally, in CS2 and CS5, the emission rate is zero because none of the energy sources produces pollution. Furthermore, the NSGA-II algorithm performed better than MOPSO, and among the five different systems designed, PV/ WT/ Battery/ EV is the most suitable case.

5.5. Conclusions and future works

This study has investigated different types of backup options for PV,WT, and battery model for three goals by using two distinct algorithms. Further, RES such as wind and solar,demand load, and EV driver's behavior were considered as uncertainties when implementing DRP.

The main outcomes of this suggested research are given below:

- ✓ MOPSO and NSGA-II algorithms were used to design and optimize five different cases to decrease LCC, LPSP, and CO_2. Simulation outcomes convey that the NSGA-II algorithm more efficient results than MOPSO. Further, it is clear that PV/ WT/ Battery/ EV collaboration is the most suitable among five different system designs.
- ✓ In this study, an EV as the backup was compared with other PV/ WT/ battery system backup modes and examined the performances in each objectives. In fact, the best LCC from both algorithms is related to CS4, while the best LPSP is related to the CS1 which is obtained from NSGA-II, and in terms of CO_2, CS2 and CS5 are the best options.

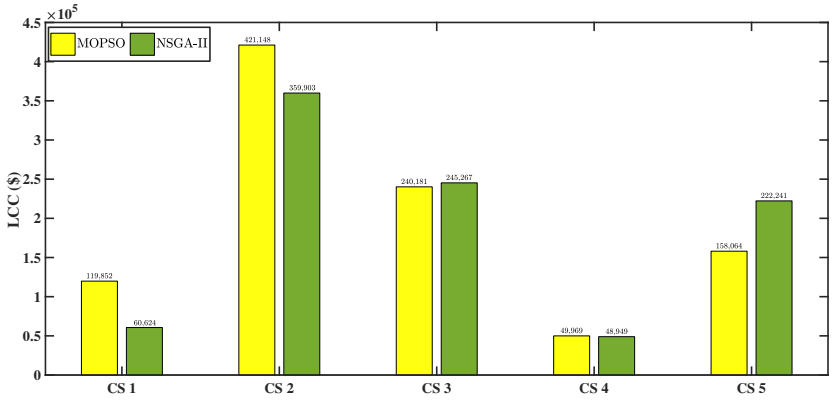

(a) LCC

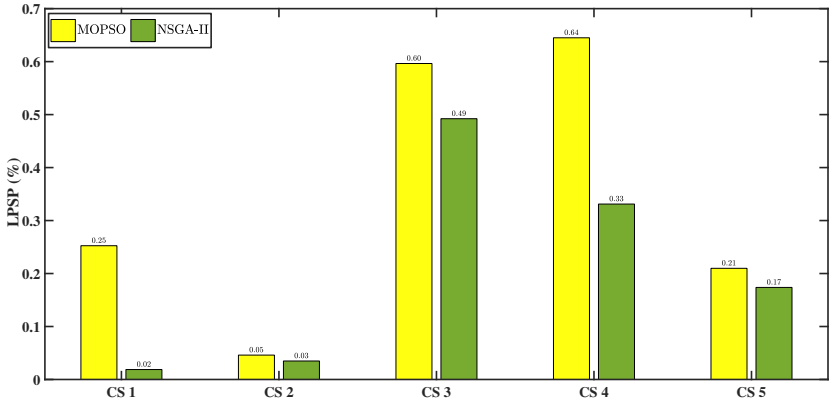

(b) LPSP

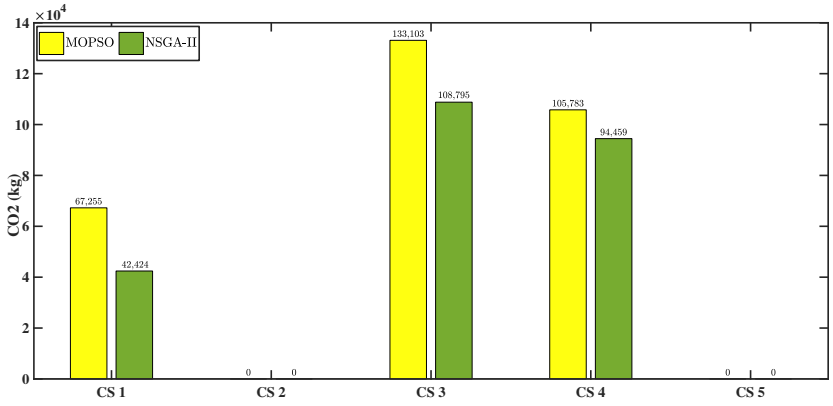

(c) CO_2

Figure 28: Comparison of (a) LCC, (b) LPSP, and (c) CO_2

- ✓ Uncertainties in wind speed, solar irradiance, and load were modeled using the three-level Taguchi method which produces 9 different scenarios. In the simulation, only the first scenario is used due to time constraints, which states that (Low, Low, and Low) or (1, 1, and 1). Further, the uncertainty has made the results more accurate.
- ✓ The EV's random functioning was designed utilizing MCS, which shows several frameworks to evaluate the arrival and departure time, and the SOC during entry to observe the irregular functioning of the EV. Moreover, the effect of EV's stochastic behavior has been considered on the number of optimal components.
- ✓ In CS4, the DRP based on TOU price was implemented, and its impact on HRES size optimization was investigated. Therefore, this case has the most optimal LCC obtained from the NSGA-II algorithm compared to other cases in the same LPSP (LPSP $= 0$) which includes 6 WT and 1 battery. Hence, the results show that the implementation of this program has a significant impact on reducing LCC.

The further studies and the subsequent ideas are highlighted below:

- ✓ The proposed system could be improved by applying other energy resources.
- ✓ Apply all the Taguchi scenarios in simulations and compare them to achieve the most accurate results.
- ✓ Other techniques and mechanisms could be include except MOPSO and NSGA-II algorithms.

6. Acknowledgment

The Authors acknowledge the support provided by King Abdullah City for Atomic and Renewable Energy (K.A.CARE) under K.A.CARE-King Abdulaziz University Collaboration Program. The authors are also thankful to Deanship of Scientific Research, King Abdulaziz University for providing financial support vide grant number (RG-37-135-42).

References

[1] S. E. Ahmadi, N. Rezaei, A new isolated renewable based multi microgrid optimal energy management system considering uncertainty and demand response, International Journal of Electrical Power & Energy Systems 118 (2020) 105760.

[2] S. E. Ahmadi, N. Rezaei, H. Khayyam, Energy management system of networked microgrids through optimal reliability-oriented day-ahead self-healing scheduling, Sustainable Energy, Grids and Networks 23 (2020) 100387.

[3] A. Mansour-Saatloo, Y. Pezhmani, M. A. Mirzaei, B. Mohammadi-Ivatloo, K. Zare, M. Marzband, A. Anvari-Moghaddam, Robust decentralized optimization of multi-microgrids integrated with power-to-x technologies, Applied Energy 304 (2021) 117635.

[4] S. E. Ahmadi, N. Rezaei, An igdt-based robust optimization model for optimal operational planning of cooperative microgrid clusters: A normal boundary intersection multi-objective approach, International Journal of Electrical Power & Energy Systems 127 (2021) 106634.

[5] M. Shabani, E. Dahlquist, F. Wallin, J. Yan, Techno-economic comparison of optimal design of renewable-battery storage and renewable micro pumped hydro storage power supply systems: A case study in sweden, Applied Energy 279 (2020) 115830.

[6] S. M. Kazemi-Razi, H. Askarian Abyaneh, H. Nafisi, Z. Ali, M. Marzband, Enhancement of flexibility in multi-energy microgrids considering voltage and congestion improvement: Robust thermal comfort against reserve calls, Sustainable Cities and Society 74 (2021) 103160.

[7] H. Schlör, S. Venghaus, J.-F. Hake, The few-nexus city index–measuring urban resilience, Applied energy 210 (2018) 382–392.

[8] M. Gharibi, A. Askarzadeh, Technical and economical bi-objective design of a grid-connected photovoltaic/diesel generator/fuel cell energy system, Sustainable Cities and Society 50 (2019) 101575.

[9] S. Zeynali, N. Nasiri, M. Marzband, S. N. Ravadanegh, A hybrid robust-stochastic framework for strategic scheduling of integrated wind farm and plug-in hybrid electric vehicle fleets, Applied Energy 300 (2021) 117432.

[10] Moghaddam, Mohammad Jafar Hadidian and Kalam, Akhtar and Nowdeh, Saber Arabi and Ahmadi, Abdollah and Babanezhad, Manoochehr and Saha, Sajeeb, Optimal sizing and energy management of stand-alone hybrid photovoltaic/wind system based on hydrogen storage considering LOEE and LOLE reliability indices using flower pollination algorithm, Renewable energy 135 (2019) 1412–1434.

[11] Mahmoudi, Sayyed Mostafa and Maleki, Akbar and Ochbelagh, Dariush Rezaei, Optimization of a hybrid energy system with/without considering back-up system by a new technique based on fuzzy logic controller, Energy Conversion and Management 229 (2021) 113723.

[12] Maleki, Akbar and Nazari, Mohammad Alhuyi and Pourfayaz, Fathollah, Harmony search optimization for optimum sizing of hybrid solar schemes based on battery storage unit, Energy Reports 6 (2020) 102–111.

[13] Arabi-Nowdeh, Saber and Nasri, Shohreh and Saftjani, Parvin Barat and Naderipour, Amirreza and Abdul-Malek, Zulkurnain and Kamyab, Hesam and Jafar-Nowdeh, Ali, Multi-criteria optimal design of hybrid clean energy system with battery storage considering off-and on-grid application, Journal of Cleaner Production 290 (2021) 125808.

[14] B. Faridpak, M. Farrokhifar, A. Alahyari, M. Marzband, A mixed epistemic-aleatory stochastic framework for the optimal operation of hybrid fuel stations, IEEE Transactions on Vehicular Technology 70 (10) (2021) 9764–9774.

[15] Abd El-Sattar, Hoda and Sultan, Hamdy M and Kamel, Salah and Menesy, Ahmed S and Rahmann, Claudia, Optimal Design of Hybrid Stand-alone Microgrids Using Tunicate Swarm Algorithm, in: 2021 IEEE International Conference on Automation/XXIV Congress of the Chilean Association of Automatic Control (ICA-ACCA), IEEE, 2021, pp. 1–6.

[16] Patibandla, Anilkumar and Kollu, Ravindra and Rayapudi, Srinivasa Rao and Manyala, Ramalinga Raju, A multi-objective approach for the optimal design of a standalone hybrid renewable energy system, International Journal of Energy Research 45 (12) (2021) 18121–18148.

[17] Zhang, Weiping and Maleki, Akbar and Pourfayaz, Fathollah and Shadloo, Mostafa Safdari, An artificial intelligence approach to optimization of an off-grid hybrid wind/hydrogen system, International Journal of Hydrogen Energy 46 (24) (2021) 12725–12738.

[18] Jahannoosh, Mariye and Nowdeh, Saber Arabi and Naderipour, Amirreza and Kamyab, Hesam and Davoudkhani, Iraj Faraji and Klemeš, Jiří Jaromír, New hybrid meta-heuristic algorithm for reliable and cost-effective designing of photovoltaic/wind/fuel cell energy system considering load interruption probability, Journal of Cleaner Production 278 (2021) 123406.

[19] D. Sadeghi, A. H. Naghshbandy, S. Bahramara, Optimal sizing of hybrid renewable energy systems in presence of electric vehicles using multi-objective particle swarm optimization, Energy 209 (2020) 118471.

[20] N. J. Vickers, Animal communication: when i'm calling you, will you answer too?, Current biology 27 (14) (2017) R713–R715.

[21] A. Maleki, M. A. Nazari, F. Pourfayaz, Harmony search optimization for optimum sizing of hybrid solar schemes based on battery storage unit, Energy Reports 6 (2020) 102–111.

[22] M. H. Jahangir, S. Fakouriyan, M. A. V. Rad, H. Dehghan, Feasibility study of

on/off grid large-scale pv/wt/wec hybrid energy system in coastal cities: A case-based research, Renewable Energy 162 (2020) 2075–2095.

[23] N. Alshammari, J. Asumadu, Optimum unit sizing of hybrid renewable energy system utilizing harmony search, jaya and particle swarm optimization algorithms, Sustainable Cities and Society 60 (2020) 102255.

[24] A. Shahkamrani, H. Askarian-abyaneh, H. Nafisi, M. Marzband, A framework for day-ahead optimal charging scheduling of electric vehicles providing route mapping: Kowloon case study, Journal of Cleaner Production 307 (2021) 127297.

[25] M. Gharibi, A. Askarzadeh, Size optimization of an off-grid hybrid system composed of photovoltaic and diesel generator subject to load variation factor, Journal of Energy Storage 25 (2019) 100814.

[26] D. Brounen, N. Kok, J. M. Quigley, Energy literacy, awareness, and conservation behavior of residential households, Energy Economics 38 (2013) 42–50.

[27] M. H. Jahangir, A. Shahsavari, M. A. V. Rad, Feasibility study of a zero emission pv/wind turbine/wave energy converter hybrid system for stand-alone power supply: A case study, Journal of Cleaner Production 262 (2020) 121250.

[28] M. Jahannoush, S. A. Nowdeh, Optimal designing and management of a stand-alone hybrid energy system using meta-heuristic improved sine–cosine algorithm for recreational center, case study for iran country, Applied Soft Computing 96 (2020) 106611.

[29] A. Ogunjuyigbe, T. Ayodele, O. Akinola, Optimal allocation and sizing of pv/wind/split-diesel/battery hybrid energy system for minimizing life cycle cost, carbon emission and dump energy of remote residential building, Applied Energy 171 (2016) 153–171.

[30] A. L. Bukar, C. W. Tan, K. Y. Lau, Optimal sizing of an autonomous photovoltaic/wind/battery/diesel generator microgrid using grasshopper optimization algorithm, Solar Energy 188 (2019) 685–696.

[31] A. Q. Mohammed, K. A. Al-Anbarri, R. M. Hannun, Optimal combination and sizing of a stand–alone hybrid energy system using a nomadic people optimizer, IEEE Access 8 (2020) 200518–200540.

[32] S. M. Mahmoudi, A. Maleki, D. R. Ochbelagh, Optimization of a hybrid energy system with/without considering back-up system by a new technique based on fuzzy logic controller, Energy Conversion and Management 229 (2021) 113723.

[33] V. Suresh, M. Muralidhar, R. Kiranmayi, Modelling and optimization of an off-grid hybrid renewable energy system for electrification in a rural areas, Energy Reports 6 (2020) 594–604.

[34] O. Ekren, C. H. Canbaz, Ç. B. Güvel, Sizing of a solar-wind hybrid electric vehicle charging station by using homer software, Journal of Cleaner Production 279 (2021) 123615.

[35] A. Razmjoo, L. G. Kaigutha, M. V. Rad, M. Marzband, A. Davarpanah, M. Denai, A technical analysis investigating energy sustainability utilizing reliable renewable energy sources to reduce co2 emissions in a high potential area, Renewable Energy (2020).

[36] A. Cano, P. Arévalo, F. Jurado, Energy analysis and techno-economic assessment of a hybrid pv/hkt/bat system using biomass gasifier: Cuenca-ecuador case study, Energy 202 (2020) 117727.

[37] M. Baseer, A. Alqahtani, S. Rehman, Techno-economic design and evaluation of hybrid energy systems for residential communities: Case study of jubail industrial city, Journal of Cleaner Production 237 (2019) 117806.

[38] S. Mandal, B. K. Das, N. Hoque, Optimum sizing of a stand-alone hybrid energy system for rural electrification in bangladesh, Journal of Cleaner Production 200 (2018) 12–27.

[39] M. Samy, M. I. Mosaad, S. Barakat, Optimal economic study of hybrid pv-wind-fuel cell system integrated to unreliable electric utility using hybrid search optimization technique, International Journal of Hydrogen Energy (2020).

[40] J. Abushnaf, A. Rassau, Impact of energy management system on the sizing of a grid-connected pv/battery system, The Electricity Journal 31 (2) (2018) 58–66.

[41] M. A. Mohamed, A. M. Eltamaly, A. I. Alolah, Swarm intelligence-based optimization of grid-dependent hybrid renewable energy systems, Renewable and Sustainable Energy Reviews 77 (2017) 515–524.

[42] M. Samy, S. Barakat, H. Ramadan, A flower pollination optimization algorithm for an off-grid pv-fuel cell hybrid renewable system, international journal of hydrogen energy 44 (4) (2019) 2141–2152.

[43] A. M. Alzahrani, M. Zohdy, B. Yan, An overview of optimization approaches for operation of hybrid distributed energy systems with photovoltaic and diesel turbine generator, Electric Power Systems Research 191 (2021) 106877.

[44] H. M. Ridha, C. Gomes, H. Hizam, M. Ahmadipour, A. A. Heidari, H. Chen, Multi-objective optimization and multi-criteria decision-making methods for optimal design of standalone photovoltaic system: A comprehensive review, Renewable and Sustainable Energy Reviews 135 (2021) 110202.

[45] N. Gholizadeh, M. Abedi, H. Nafisi, M. Marzband, A. Loni, G. A. Putrus, Fair-optimal bilevel transactive energy management for community of microgrids, IEEE Systems Journal (2021) 1–11.

[46] Y. Xu, C. Yan, H. Liu, J. Wang, Z. Yang, Y. Jiang, Smart energy systems: A critical review on design and operation optimization, Sustainable Cities and Society (2020) 102369.

[47] M. S. Jonban, L. Romeral, A. Akbarimajd, Z. Ali, S. S. Ghazimirsaeid, M. Marzband, G. Putrus, Autonomous energy management system with self-

healing capabilities for green buildings (microgrids), Journal of Building Engineering 34 (2021) 101604.

[48] C. Li, D. Zhou, H. Wang, Y. Lu, D. Li, Techno-economic performance study of stand-alone wind/diesel/battery hybrid system with different battery technologies in the cold region of china, Energy 192 (2020) 116702.

[49] A. Maleki, M. Gholipour, M. Ameri, Electrical power and energy systems optimal sizing of a grid independent hybrid renewable energy system incorporating resource uncertainty, and load uncertainty, Int. J. Electr. Power Energy Syst 83 (2016) 514–524.

[50] Ö. F. Ertugrul, Forecasting electricity load by a novel recurrent extreme learning machines approach, International Journal of Electrical Power & Energy Systems 78 (2016) 429–435.

[51] K. Ndwali, J. G. Njiri, E. M. Wanjiru, Multi-objective optimal sizing of grid connected photovoltaic batteryless system minimizing the total life cycle cost and the grid energy, Renewable Energy 148 (2020) 1256–1265.

[52] L. jing Hu, K. Liu, Y. Fu, P. Li, Capacity optimization of wind/pv/storage power system based on simulated annealing-particle swarm optimization, in: 2018 37th Chinese Control Conference (CCC), IEEE, 2018, pp. 2222–2227.

[53] R. Goddard, L. Zhang, X. Xia, Optimal sizing and power sharing of distributed hybrid renewable energy systems considering socio-demographic factors, Energy Procedia 159 (2019) 340–345.

[54] R. Wang, G. Li, M. Ming, G. Wu, L. Wang, An efficient multi-objective model and algorithm for sizing a stand-alone hybrid renewable energy system, Energy 141 (2017) 2288–2299.

[55] N. Ghorbani, A. Kasaeian, A. Toopshekan, L. Bahrami, A. Maghami, Optimizing a hybrid wind-pv-battery system using ga-pso and mopso for reducing cost and increasing reliability, Energy 154 (2018) 581–591.

[56] Greenhouse gas emission intensity of electricity generation by country @ONLINE, Published 25 Oct 2021 (2021).
URL https://www.eea.europa.eu/data-and-maps/

[57] H. Aalami, M. P. Moghaddam, G. Yousefi, Demand response modeling considering interruptible/curtailable loads and capacity market programs, Applied Energy 87 (1) (2010) 243–250.

[58] S. Yousefi, M. P. Moghaddam, V. J. Majd, Optimal real time pricing in an agent-based retail market using a comprehensive demand response model, Energy 36 (9) (2011) 5716–5727.

[59] M. Kharrich, O. H. Mohammed, N. Alshammari, M. Akherraz, Multi-objective optimization and the effect of the economic factors on the design of the microgrid hybrid system, Sustainable Cities and Society 65 (2021) 102646.

[60] R. Wang, J. Xiong, M.-f. He, L. Gao, L. Wang, Multi-objective optimal design of hybrid renewable energy system under multiple scenarios, Renewable Energy 151 (2020) 226–237.

[61] M. Marzband, M. Javadi, J. L. Domínguez-García, M. M. Moghaddam, Non-cooperative game theory based energy management systems for energy district in the retail market considering der uncertainties, IET Generation, Transmission & Distribution 10 (12) (2016) 2999–3009.

[62] F. Y. Melhem, O. Grunder, Z. Hammoudan, N. Moubayed, Optimization and energy management in smart home considering photovoltaic, wind, and battery storage system with integration of electric vehicles, Canadian Journal of Electrical and Computer Engineering 40 (2) (2017) 128–138.

[63] M.-H. Wang, M.-L. Huang, Z.-Y. Zhan, C.-J. Huang, Application of the extension taguchi method to optimal capability planning of a stand-alone power system, Energies 9 (3) (2016) 174.

[64] Solar radiation and wind speed resources, accessed: 01.09.2019 (2021).
URL https://www.pecanstreet.org/dataport/

[65] P. Aliasghari, B. Mohammadi-Ivatloo, M. Alipour, M. Abapour, K. Zare, Optimal scheduling of plug-in electric vehicles and renewable micro-grid in energy and reserve markets considering demand response program, Journal of Cleaner Production 186 (2018) 293–303.